GCM simulations of anthropogenic aerosol-induced changes in aerosol extinction, atmospheric heating and precipitation over India

Ribu Cherian,[1,2,4] C. Venkataraman,[1] J. Quaas,[2] and S. Ramachandran[3]

Received 23 July 2012; revised 11 February 2013; accepted 21 February 2013; published 15 April 2013.

[1] The influence of anthropogenic emissions on aerosol distributions and the hydrological cycle are examined with a focus on monsoon precipitation over the Indian subcontinent, during January 2001 to December 2005, using the European Centre for Medium-Range Weather Forecasts-Hamburg (ECHAM5.5) general circulation model extended by the Hamburg Aerosol Module (HAM). The seasonal variability of aerosol optical depth (AOD) retrieved from the MODerate Resolution Imaging Spectroradiometer (MODIS) on board the Terra and Aqua satellite is broadly well simulated ($R \approx 0.6$–0.85) by the model. The spatial distribution and seasonal cycle of the precipitation observed over the Indian region are reasonably well simulated ($R \approx 0.5$ to 0.8) by the model, while in terms of absolute magnitude, the model underestimates precipitation, in particular in the south-west (SW) monsoon season. The model simulates significant anthropogenic aerosol-induced changes in clear-sky net surface solar radiation (dimming greater than -7 W m^{-2}), which agrees well with the observed trends over the Indian region. A statistically significant decreasing precipitation trend is simulated only for the SW monsoon season over the central-north Indian region, which is consistent with the observed seasonal trend over the Indian region. In the model, this decrease results from a reduction in convective precipitation, where there is an increase in stratiform cloud droplet number concentration (CDNC) and solar dimming that resulted from increased stability and reduced evaporation. Similarities in spatial patterns suggest that surface cooling, mainly by the aerosol indirect effect, is responsible for this reduction in convective activity. When changes in large-scale dynamics are allowed by slightly disturbing the initial state of the atmosphere, aerosol absorption in addition leads to a further stabilization of the lower troposphere, further reducing convective precipitation.

Citation: Cherian, R., C. Venkataraman, J. Quaas, and S. Ramachandran (2013), GCM simulations of anthropogenic aerosol-induced changes in aerosol extinction, atmospheric heating and precipitation over India, *J. Geophys. Res. Atmos.*, *118*, 2938–2955, doi:10.1002/jgrd.50298.

1. Introduction

[2] Atmospheric aerosols play a significant role in the global and regional climate system by influencing the energy balance of the atmosphere and the Earth's surface, thus modulating the hydrological cycle [*Ramanathan et al*., 2005]. The large spatiotemporal variation not only of their atmospheric concentrations, but also of their physical and chemical properties makes the climatic effects of aerosols highly uncertain [*Forster et al*., 2007]. The indirect effects of atmospheric aerosols (i.e., through modification of cloud properties and precipitation processes) are one of the least understood forcings of climate change [*Forster et al*., 2007]. Recent studies suggest that aerosols may be effective agents for inducing changes in monsoon precipitation [*Ramanathan et al*., 2005; *Lau et al*., 2006]. However, different mechanisms are discussed and even the sign of precipitation changes induced by anthropogenic aerosols is disputed.

[3] General circulation model (GCM) studies suggested that anthropogenic aerosols could influence monsoon precipitation patterns over South Asia [*Ramanathan et al*., 2005; *Meehl et al*., 2008] and East Asia [*Menon et al*., 2002]. Recent studies suggest that aerosols may affect precipitation patterns by decreasing the frequency of drizzle (cloud lifetime effect), while increasing the intensity of heavy, convective, rainfall via the "convective invigoration" hypothesis [*Andreae et al*., 2004; *Andreae and Rosenfeld*, 2008]. GCM studies of the direct and semi-direct effects of absorbing aerosols have found that widespread regional aerosol atmospheric heating may influence the precipitation patterns in the early part of the monsoon season over the Indian region [*Lau et al*., 2006; *Randles*

All supporting information may be found in the online version of this article

[1]Department of Chemical Engineering, Indian Institute of Technology Bombay, Mumbai, India.
[2]Max Planck Institute for Meteorology, Hamburg, Germany.
[3]Physical Research Laboratory, Ahmedabad, India.
[4]Institute for Meteorology, Universität Leipzig, Leipzig, Germany.

Corresponding author: R. Cherian, Institute for Meteorology, Universität Leipzig, Stephanstr. 3, D-04103 Leipzig, Germany. (ribu.cherian@uni-leipzig.de)

2169-897X/13/10.1002/jgrd.50298

and Ramaswamy, 2008]. Absorbing aerosols alter the spatial gradient in the atmospheric heating and this alteration may perturb the spatial distribution and timing of monsoonal rainfall in South Asia, with more rain in some regions and less in others [*Menon et al*., 2002]. *Ramanathan et al*. [2005] also found that aerosols (mainly black carbon and sulfate) might have played a major role in the regional-scale reduction of rainfall through the solar dimming and surface cooling effects, as sulfate directly scatters sunlight and both aerosols modify cloud reflectivity when acting as cloud condensation nuclei. In a GCM study, *Lau et al*. [2006] investigated elevated atmospheric heating by absorbing aerosols and the effects on the rainfall distribution of the monsoon system (the "elevated heat pump" hypothesis attributed to dust and black carbon) and found this to potentially increase precipitation in the early part of the summer monsoon season (May–June). Observational studies based on long-term (1979–2007) tropospheric temperature trends showed a widespread warming trend over the Himalayan-Gangetic region and consequent strengthening of the land-sea thermal gradient that support the elevated heat pump hypothesis [*Gautam et al*., 2009; *Lau and Kim*, 2010]. However, an assessment using satellite aerosol retrievals did not support the strong "elevated" solar heating over the Tibetan Plateau region [*Kuhlmann and Quaas*, 2010]. It is thus not clear how aerosols influence the monsoon water cycle on seasonal-to-interannual time scales.

[4] Studies analyzing the trends in observed summer monsoon rainfall over the Indian region show spatial patterns with trends of different magnitudes and of both signs [*Dash et al*., 2009; *Ghosh et al*., 2009]. The frequency of occurrence of heavy-intensity precipitation events has been found to increase in the Indo-Gangetic Plain (IGP), while for northeastern India, a reduction of the frequency of occurrence of light or moderate precipitation has been reported [*Dash et al*., 2009; *Goswami et al*., 2006]. These trends have implications for society. An increase in heavy precipitation can lead to more and worse floods and landslides, while a decrease of light or moderate precipitation events, which frequently occur in different seasons, poses serious drought problems [*Dash et al*., 2009]. These trends are not only results from changes in large scale meteorological parameters, but may also be influenced by the changes in regional aerosol loading. These studies point out the necessity of aerosol-climate modeling studies for better understanding of aerosol-cloud-precipitation interactions. Especially over the Indian region, this could offer a better understanding of how technology and human actions, through emissions, impact atmospheric heating and precipitation patterns.

[5] The main aim of the present study is to assess the direct and indirect effects of anthropogenic aerosols on South Asian climate, with a focus on precipitation over the Indian region. The objectives of the present study are (a) understand the influence of anthropogenic aerosols on seasonal rainfall patterns using a general circulation model (the European Centre for Medium-Range Weather Forecasts (ECMWF) Hamburg model, ECHAM, version 5.5, extended by the Hamburg aerosol module, HAM), (b) investigate the effects of anthropogenic aerosols on aerosol loading, and (c) understand the influence of atmospheric large-scale circulation patterns on aerosol-induced precipitation changes over the Indian region (section 4.2.4). In this study, the simulations were not appropriate to gain insight into the actual time evolution of the aerosol loading and climate response to anthropogenic aerosol emissions. Transient changes in anthropogenic aerosols were not considered, rather, present-day anthropogenic aerosol emissions are kept constant at year 2000 level. Also, it should be emphasized that the present study only addresses anthropogenic aerosol effects on the mean climatology, rather than on weather effects. Experience shows that the 5 years considered are sufficient [*Lohmann and Hoose*, 2009] to obtain a good signal-to-noise ratio in the identification of climatic impacts since sea surface temperatures are prescribed.

[6] This paper is organized as follows. Section 2 describes the model, data sets, and analysis method. The simulation setup and aerosol emission inventory details are explained in section 3. The influence of anthropogenic aerosol emissions on aerosol loading and the climate effects are discussed in section 4. The main findings are summarized in section 5.

2. Methodology and Data Sets

[7] The ability of climate models to accurately simulate features of the Indian summer monsoon is crucial for building confidence in future model projections of precipitation response to climate forcing. Climate models that adequately reproduce observed temporal cycles in large-scale features (land-ocean temperature contrast/pressure gradient and wind circulation patterns) may have a higher degree of credibility in simulating anthropogenic precipitation perturbations [*Kripalani et al*., 2007; *Annamalai et al*., 2007]. Recent model intercomparison studies found that the ECHAM model (ECHAM5/Max Planck Institute Ocean Model (MPI-OM)) provided the closest agreement with the observed seasonal, annual, and interannual cycle and magnitudes of the Indian summer monsoon precipitation [*Kripalani et al*., 2007; *Annamalai et al*., 2007]. In addition, the ECHAM model reproduces well the observed El Niño-Southern Oscillation-related SST variability, land-ocean pressure gradient, and the observed SST and rainfall connection [*Kripalani et al*., 2007; *Annamalai et al*., 2007].

[8] The influence of anthropogenic aerosols on seasonal monsoon rainfall patterns was investigated using present-day (PD, 2000) and pre-industrial (PI, 1750) anthropogenic aerosol emission inventories. A new, regionally validated anthropogenic aerosol emission data set for PD emissions was used (section 3), with better model resolution of 180 km compared to previous studies (≥300 km) [e.g. *Menon et al*., 2002; *Ramanathan et al*., 2005], more detailed cloud microphysics description (section 2.1), and a realistic mix of natural and anthropogenic aerosols (section 2.1). The model-simulated aerosol optical depth (AOD) and precipitation patterns were evaluated seasonally using satellite retrievals. A seasonal-mean trend analysis averaged for 5 years for the period 2001–2005 was performed for model-simulated aerosol distributions, radiative effects, atmospheric heating patterns, and monsoon precipitation.

2.1. Model Description

[9] Atmospheric simulations were made with the ECHAM5.5 GCM [*Roeckner et al*., 2003] with a horizontal resolution of T63 (about $1.8° \times 1.8°$) and a vertical resolution of 31 levels (extended from the surface to 10 hPa) combined with the aerosol module HAM [*Stier et al*., 2005]. The main components of HAM are the microphysical module M7,

which predicts the evolution of an ensemble of seven internally mixed lognormal aerosol modes [*Vignati et al*., 2004], an emission module, a sulfate chemistry scheme [*Feichter et al*., 1996], a deposition module, and a radiative transfer module [*Stier et al*., 2005; *Stier et al*., 2007] to account for sources, transport, and sinks of aerosols as well as their radiative impact. The governing equations for mass and number concentrations in the respective size/solubility classes are solved for five aerosol components namely sulfate, black carbon (BC), organic carbon (OC), sea salt, and mineral dust. Emissions of sea salt are calculated by using the simulated wind speed at 10 m height, snow cover, SST, and sea ice cover. In the model, mineral dust emissions are calculated based on the online prognostic wind speed at 10 m height and the prescribed surface features of soils [*Stier et al*., 2005]. The anthropogenic emissions of SO_2, BC, and OC are prescribed (see section 3).

[10] In the model, the convective and stratiform (large-scale) precipitation is estimated separately through cumulus convection and large-scale precipitation parameterizations. For cumulus convection (shallow, mid-level, and deep), a bulk mass flux scheme [*Tiedtke*, 1989] is employed with modifications for deep convection according to *Nordeng* [1994]. The scheme is based on steady state equations for mass, heat, moisture, cloud water, and momentum for an ensemble of updrafts and downdrafts, including turbulent and organized entrainment and detrainment. Cloud water detrainment in the upper part of convective updrafts is used as a source term in the stratiform cloud water equations [*Hagemann et al*., 2006]. The microphysics for convective clouds follows the coarse parameterization by *Tiedtke* [1989] where no effects of aerosols are taken into account.

[11] The stratiform cloud scheme consists of prognostic equations for the water phases (vapor, liquid, and solid), two-moment cloud microphysics [*Lohmann et al*., 2007], with aerosol effects on clouds taken into account for liquid-water clouds. The statistical cloud cover scheme has prognostic equations for the distribution moments [*Tompkins*, 2002]. The microphysics scheme includes phase changes between the water components (condensation/evaporation, deposition/sublimation, and freezing/melting) and precipitation processes (auto-conversion, accretion, and aggregation). Moreover, the evaporation of rain and the melting of snow are considered, as well as the sedimentation of cloud ice [*Hagemann et al*., 2006]. The effect of aerosols on stratiform clouds is parameterized using a two-moment prognostic cloud microphysical scheme, which predicts both the mass-mixing ratio and number concentration of cloud droplets and ice crystals [*Lohmann et al*., 2007]. In this scheme, aerosols serve as cloud condensation nuclei for liquid-water clouds. No effect on ice clouds is included, since theoretical and modeling studies using the ECHAM5-HAM GCM have shown that homogeneous nucleation is dominant (at temperatures less than −38°C) [*Lohmann et al*., 2008], i.e., ice crystal concentrations are formed via this mechanism only.

2.2. Data Sets

[12] The daily Level 3 MODIS (collection V005) global $1° \times 1°$ gridded AOD at 550 nm from both Terra (approximate local overpass time at about 10.30 local standard time (LST)) and Aqua (overpass at 13.30 LST) satellites was averaged to obtain daily average and used to evaluate the model-simulated AOD. The daily accumulated $0.25° \times 0.25°$ rainfall product (beginning at 00Z and ending at 21Z) over the global tropics (40°N-40°S) from the Tropical Rainfall Measuring Mission (TRMM) was used to evaluate the model-simulated precipitation fields in this study. The rainfall measuring instruments on the TRMM satellite include the Precipitation Radar (PR), an electronically scanning radar operating at 13.8 GHz; the TRMM Microwave Image (TMI), a nine-channel passive microwave radiometer; and the Visible and Infrared Scanner (VIRS), a five-channel visible/infrared radiometer [*Huffman et al*., 2007]. The daily mean (03-03 Z, LST) rainfall data ($0.5° \times 0.5°$) product [*Rajeevan et al*., 2006] provided by the Indian Meteorological Department (IMD) is also used to evaluate the model-simulated precipitation fields over the Indian region.

3. Simulation Setup and Approach

[13] In this study, the model simulations were performed with prescribed present-day climatological observed sea surface temperature (SST) and sea ice concentration (SIC) using the monthly varying Atmospheric Model Intercomparison Project (AMIP) data sets, and with prescribed present-day long-lived greenhouse gas concentrations, ozone, and land-surface properties. The simulations differ only in the emissions of anthropogenic aerosol and aerosol precursor gases (BC, OC, and SO_2). In the control run, the PI (1750) anthropogenic aerosol emission inventory is used, while in the experiment simulation the PD anthropogenic aerosol emissions are used (see Table 1). In both PD and PI runs, we performed nudged simulations, in which the model prognostic variables, namely vorticity, divergence, temperature, and pressure, were relaxed toward the ECMWF re-analysis data based on a Newtonian relaxation technique [*Jeuken et al*., 1996]. The relaxation time scales used for nudging in the prognostic equations are 48 h for divergence, 6 h for vorticity, 24 h for temperature, and 24 h for surface pressure. To analyze the effect of atmospheric circulation changes, an ensemble of three non-nudged simulations was also carried out for both PI and PD aerosol emissions. Three ensemble members were generated by slightly disturbing the model parameter (by slightly multiplying the coefficients for horizontal diffusion for divergence, vorticity, and temperature with a factor

Table 1. Summary of Simulation Setup and Emission Data Sets Used in This Study

Experiment Name	Simulated Years	Prescribed Emissions (DMS, dust, and sea salt are calculated interactively based on the meteorology and surface properties)
Pre-industrial (PI)	5 years (2001–2005)	1750 anthropogenic emissions [*Dentener et al*., 2006]
Present-day (PD)	5 years (2001–2005)	SO_2, BC, and OC (AEROCOM [*Dentener et al*., 2006] + REGIONAL INDIAN EMISSION INVENTORY [*Reddy and Venkataraman*, 2002; *Venkataraman et al*., 2006]) fixed at year 2000 levels

1.0001, 0.9999, or 1.0000), a modification which did not influence the simulated climate but only generates a different weather distribution. The ensemble mean of the non-nudged simulations is used for the analysis.

[14] In this study, the prescribed SSTs and SICs were used to isolate and examine the effects of anthropogenic aerosols on the atmospheric heating and precipitation patterns, without the complexity of a fully coupled ocean-atmosphere model. By applying the observed SSTs as the lower boundary condition, most of the uncertainties associated with the lower boundary forcing (which may arise from the use of a mixed layer ocean or a fully coupled ocean model) do not come into picture. The feedback of SST changes to aerosol surface cooling was not considered in this study. This is to reduce the complexity in the effects of aerosols on precipitation patterns.

[15] Aerosol emissions, based on the AEROCOM emission inventory [*Dentener et al*., 2006] for the year 2000 are combined with regional emission inventories available over India [*Reddy and Venkataraman*, 2002; *Venkataraman et al*., 2005; *Venkataraman et al*., 2006]. The combined emission data set was used for residential, transport, industry, and agricultural residue burning emission sectors. AEROCOM global emissions of SO_2 for these sectors are from *Cofala et al*. [2005] and BC and OC global emissions are from *Bond et al*. [2004]. Global fire emission data (GFED) were used for forest burning emission sectors. Volcanic emissions of SO_2 are included [*Andres and Kasgnoc*, 1998]. Dust and sea salt emissions were calculated online [*Tegen et al*., 2002] using the ECHAM 10 m wind speed. The spatial resolution used for the emission data set matches the model's horizontal resolution (T63).

[16] Each simulation covers 5 years (2001–2005) after a spin-up of 3 months to initialize aerosol fields. In this study, the seasons are defined based on the dominant aerosol types and emission sources. It is known that absorbing carbonaceous aerosols are mostly confined in the inter-monsoon (or post-monsoon, October-November; ON), north-east (NE) monsoon (December-January-February; DJF) and the pre-monsoon (March-April-May; MAM) seasons over the Indian subcontinent. During DJF, biomass burning aerosols mainly result from wildfire and residential biofuel combustion over the Indian subcontinent [*Venkataraman et al*., 2006]. During MAM and ON, agricultural crop residues are burnt over the Indian subcontinent, which has significant impact on aerosol loading. Therefore, in this study, we have selected DJF as NE monsoon, MAM as pre-monsoon, and ON as inter-monsoon seasons. Based on this, four different seasons, i.e., NE monsoon, pre-monsoon, south-west monsoon (SW, June-July-August-September; JJAS), and inter-monsoon seasons are selected for the analysis.

[17] The anthropogenic aerosol-induced change in AOD and precipitation is estimated as the differences between the experiment with the PD anthropogenic aerosol emissions and the PI anthropogenic aerosol emissions averaged for 5 years for the period from January 2001 to December 2005 (i.e., $\Delta = \mathrm{PD} - \mathrm{PI}$). The clear-sky short-wave aerosol radiative forcing (ARF) at the top of the atmosphere (TOA) and the surface (SUR) is estimated as the change in net (downward minus upward) radiative fluxes, with and without the presence of aerosols in the atmosphere as

$$F_{\mathrm{TOA,SUR}} = F_{\mathrm{withaerosolTOA,SUR}} - F_{\mathrm{withoutaerosolTOA,SUR}}. \quad (1)$$

[18] The ARF within the atmosphere is estimated as the difference between the ARF at TOA and SUR. The short-wave aerosol indirect radiative effects or cloud radiative effects are computed as the difference between all-sky and clear-sky radiative fluxes. The surface indirect radiative forcing is defined in terms of net downwelling flux as

$$F_{\mathrm{cloudy\text{-}sky}} = F_{\mathrm{all\text{-}sky}} - F_{\mathrm{clear\text{-}sky}} \quad (2)$$

where $F_{\mathrm{all\text{-}sky}}$ and $F_{\mathrm{clear\text{-}sky}}$ denote the all-sky and clear-sky net downwelling short-wave radiation fluxes, respectively. The anthropogenic aerosol-induced direct and indirect radiative forcing is then defined as the difference in direct and indirect radiative effects, respectively, between the simulations with PD and PI anthropogenic aerosol emissions.

4. Results and Discussion

4.1. Model Evaluation

4.1.1. Aerosol Optical Depth (AOD)

[19] The spatial distribution of the model-simulated PD seasonal-mean AODs averaged over 5 years (2001–2005) was evaluated using MODIS-derived Terra and Aqua satellite combined AOD values (Figure 1). The model broadly ($R \approx 0.6$ to 0.85) captures AOD distributions during all different seasons over the Indian region. During the NE monsoon season, high AOD (0.2 to 0.4) is found over the IGP (Figure S1in the auxiliary material) and central-north India (CNI), with substantially lower values (mean bias = −0.12) in the model compared to the satellite retrievals, but with a similar southwest-northeast gradient. The local maximum in AOD was previously observed from satellite retrievals [*Di Girolamo et al*., 2004; *Ramachandran and Cherian*, 2008] and ground-based observations [*Singh et al*., 2004]. The predicted northeastern maximum is from high anthropogenic emissions (mainly for sulfate and OC; Figure 2). The contribution of fine-mode aerosols, such as sulfate and OC, to the predicted AOD is dominant during the NE monsoon period (Figure 2). During the pre-monsoon season, AOD patterns change substantially (0.1–0.15) over the Indian subcontinent from an enhancement in dust loading (Figures 1 and 2). This is consistent with the findings from previous studies [*Dey et al*., 2004; *Ramachandran and Cherian*, 2008; *Gautam et al*., 2011]. High AOD is found over the IGP and CNI regions (Figure 1), but underestimated in magnitude by the model (mean bias = −0.1). The model shows a local minimum in the north-western Indian (NWI) region, where the satellite retrievals show moderate AOD values. A large influx of desert dust from the western arid and desert regions of Arabia, Africa, and Thar (Rajasthan) enhances the dust loading over these regions during the pre-monsoon season [*Dey et al*., 2004; *Dey and Girolamo*, 2010], and this dust influx may be underestimated by the model [*Cherian et al*., 2012], most likely from inaccurate representation of soil erodibility factor and soil moisture. Nevertheless, the model shows that the dust contribution to total AOD is high (30–40%) during the pre-monsoon period over the IGP and NWI regions (Figure 2). In addition to dust, SO_4 and OC show a significant contribution to total AOD over

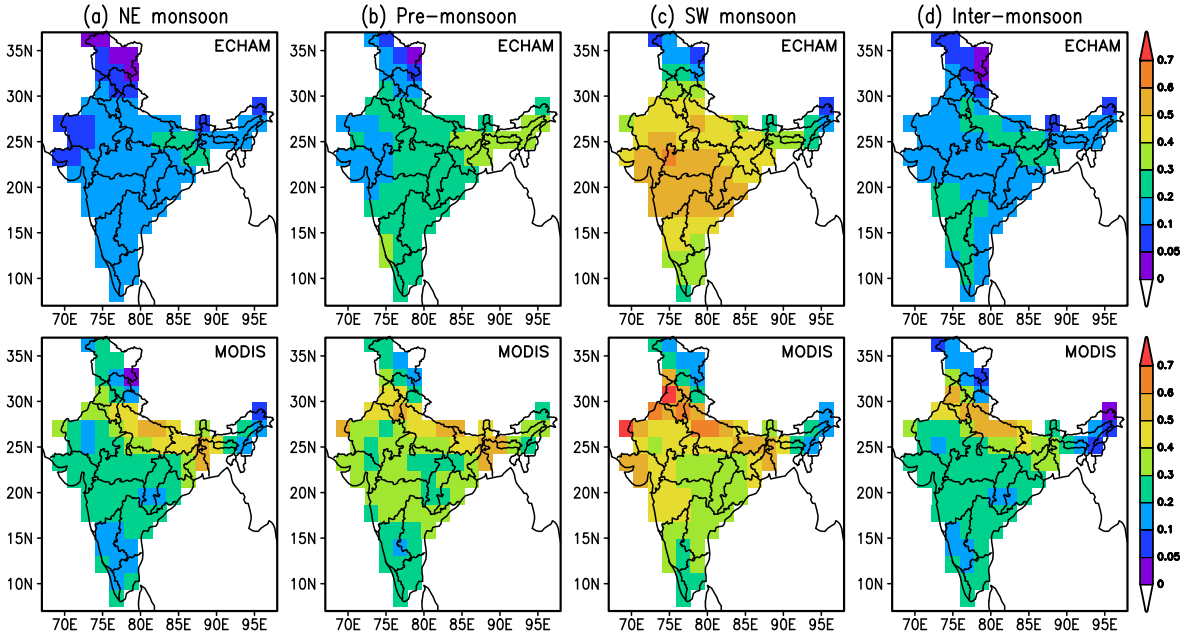

Figure 1. Seasonal-mean distribution of model-simulated present-day aerosol optical depth at 550 nm and MODIS satellite (Terra and Aqua combined) retrievals (January 2001 to December 2005; north-east monsoon (DJF), pre-monsoon (MAM), south-west monsoon (JJAS), and inter-monsoon (ON)).

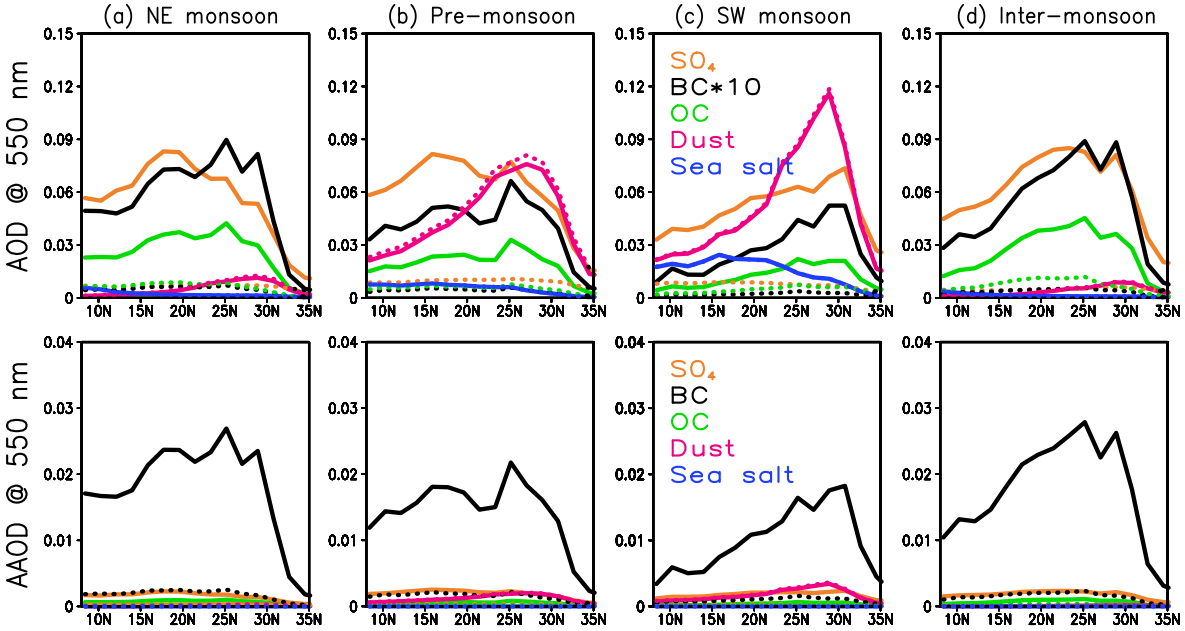

Figure 2. Seasonal zonal-mean (India, 68°E–98°E) distribution of species-wise contribution to model-simulated aerosol optical depth (AOD) and absorption aerosol optical depth (AAOD) at 550 nm (January 2001 to December 2005; north-east monsoon (DJF), pre-monsoon (MAM), south-west monsoon (JJAS), and inter-monsoon (ON)). The solid lines indicate the present-day values and dashed lines indicate the pre-industrial values.

a large part of the Indian subcontinent (Figure 2). These observations are consistent with the fact that anthropogenic aerosols also contribute significantly to AOD along with dust aerosols over these regions [*Dey and Girolamo*, 2010]. It is also known that, in addition to dust storms, open biomass burning peaks during the pre-monsoon season over these regions [*Vadrevu et al.*, 2011; *Venkataraman et al.*, 2006].

[20] In the monsoon season, high AOD values are found over the IGP, NWI, and CNI regions (Figure 1), consistently in model and satellite retrievals (mean bias = 0.04), albeit too far south-west in the GCM. This maximum arises because

of an enhanced transport of dust aerosols from desert regions of Arabia, Africa, and Thar (Rajasthan), and also of sea salt from the ocean (Figure 2). The AOD composition was found to be dominated by dust aerosols, followed by sulfate, OC, and sea salt aerosols during this season (Figure 2). It should be emphasized that during the SW monsoon months, it is cloudy and retrieval of MODIS AODs could be affected by the cloud cover. The intense cloud cover also leads to limited number of days of MODIS AOD retrievals during this period [*Ramachandran and Cherian*, 2008]. Potential retrieval artifacts, however, cannot be taken into account in the model. In the model, it may be noted that simulated AOD is computed from clear-sky relative humidity. Therefore, as a cautionary note, good agreement between model-simulated and satellite-retrieved AODs during SW monsoon season may not entirely be substantiated. During the inter-monsoon season, high AODs are found over the northern parts of the IGP (Figure 1), but underestimated in magnitude by the model (mean bias = −0.05). The composition of total AOD was dominated by sulfate followed by OC and BC aerosols during this season (Figure 2). It is known that agricultural residue and biofuel burning emissions dominate the aerosol emissions during this season [*Vadrevu et al*., 2011; *Bond et al*., 2004; *Venkataraman et al*., 2006].

[21] In summary, seasonal and spatial variability of the model-simulated AOD broadly captures the MODIS-retrieved variability over the Indian region. In particular, the model-simulated AOD was well simulated during the SW monsoon and inter-monsoon seasons (with a certain geographical displacement), but significantly underpredicted locally by up to a factor of 2 during the NE monsoon because of the uncertainties in regional emission inventories and dust emission fluxes [*Cherian et al*., 2012]. It has been shown that pre-monsoon aerosol-induced atmospheric heating may enhance the early part of the SW monsoon rainfall over the Indian region [*Lau et al*., 2006; *Randles and Ramaswamy*, 2008]. The model-simulated AOD slightly underestimates (by a factor of 1.1–1.25) the retrieved AOD over the IGP (temporal correlation coefficient of model AOD versus MODIS AOD is 0.85) during the SW monsoon season, while it slightly overestimates the AOD over the CNI by a factor of 1.25–1.5, which leads to a maximum AOD over these regions. The overestimation of AOD is likely due to the contribution of aerosol hygroscopicity of water-soluble aerosols (sulfate) over these regions. The other factors leading to AOD differences could be related to the difficulty in satellite retrievals of AOD in the monsoon season with large cloud cover. During the pre-monsoon season, the model underestimates the AOD mainly over the IGP, which results from an underestimation of dust emission fluxes over these regions [*Cherian et al*., 2012]. Similar AOD underestimations were also reported in previous model estimations [*Kinne et al*., 2003].

[22] The broad regional differences of AOD patterns over the Indian subcontinent depend on the anthropogenic (sulfate and OC) and natural (dust) emission sources, but the seasonal variation within the region depends significantly also on the meteorology (dust transport or relative humidity (RH)). Besides, the maximum underestimation of AOD (0.1–0.2 in absolute units) occurring in the NE monsoon season suggests that the problem is not mainly caused by RH biases or hygroscopicity of aerosols in the model (Figure 1). The AOD differences could also be related to production and removal of aerosols in the model. But the same discrepancy occurring in most of the aerosol-climate models using different aerosol microphysics suggests that the removal of aerosols is not the primary cause of this problem. Therefore, the noted differences between model-simulated AOD and MODIS AOD are largely caused by the problems associated with the poor characterization of dust sources over this region [*Cherian et al*., 2012] as well as the uncertainties in the anthropogenic aerosol emission inventories. The underestimation of AOD in the model could also be related to the effect of low-resolution topography, which is smoothed out in the model (180 km resolution) *Gautam et al*., 2011; *Prabha et al*., 2012].

4.1.2. Single Scattering Albedo (SSA)

[23] The response of aerosol effects on regional climate strongly depends on the SSA along with the AOD values. Uncertainties in the simulated SSA may change the sign of aerosol radiative effects and thereby precipitation changes. Here, the model-simulated SSA is evaluated using published Sun photometer observations (Table 2). The SSA at wavelength 550 nm in the ECHAM5.5-HAM model PD simulations is 0.85–0.90 over the IGP and the CNI region (Figure S2), which agrees reasonably well with previously reported SSA values [*Pandithurai et al*., 2008; *Singh et al*., 2004; *Jethva et al*., 2005; *Ganguly et al*., 2005; *Dey and Tripathi*, 2008; *Gadhavi and Jayaraman*, 2010; *Gautam et al*., 2011]. The model is also able to reproduce the seasonal-mean SSA patterns with the reported values over the northern Indian region (see Table 2 and Figure S2). This includes low SSA (0.75–0.85) over north India during the NE monsoon period and high SSA (0.92–0.98) during the SW monsoon period, which is consistent with the observed values (Table 2). However, there are differences in SSA between model and observations, which could be associated with the uncertainties in BC and dust emissions, microphysical transformation, and sinks, and likely with errors in the optical properties used in the model for the individual aerosol species. The close agreement between model-simulated SSA with the observed SSA values provides confidence in the simulated PD aerosol solar absorption and the aerosol internal mixing simulated by the model.

[24] In addition to this, the atmospheric heating response strongly depends on the vertical distribution of aerosols. A recent study showed that ECHAM5-HAM model-simulated extinction profiles agree well with profiles derived by the Cloud-Aerosol Lidar and Infrared Pathfinder Satellite Observations (CALIPSO; RMSE 0.21 and correlation coefficient 0.71 for 0–6 km altitude ranges) [*Koffi et al*., 2012], which provides greater confidence in model-simulated vertical distribution of aerosols.

4.1.3. Precipitation

[25] In this section, the spatial distribution of model-simulated seasonal-mean precipitation patterns is evaluated against IMD precipitation and TRMM satellite-derived precipitation fluxes during 2001–2005 (Figure 3). The TRMM rainfall values broadly agree ($R \approx 0.8$–0.9) with IMD-observed rainfall values in all seasons (Figure 3). The spatial distribution of mean model-simulated precipitation (mm/day) broadly captures ($R \approx 0.5$–0.8) both the IMD-observed and TRMM satellite-retrieved rainfall patterns over the Indian region in all seasons, while the magnitude of rainfall is not predicted accurately. More than 75% of the annual model-simulated rainfall over the Indian subcontinent occurs during

Table 2. Comparison of Model-Simulated Present-Day Single Scattering Albedo at 550 nm (SSA, 2001–2005 Mean) With Reported Values in Different Seasons

Region	NE monsoon (DJF)		Pre-monsoon (MAM)		SW monsoon (JJAS)		Inter-monsoon (ON)		Annual	
	Present study at 550 nm	Previous study	Present study at 550 nm	Previous study	Present study at 550 nm	Previous study	Present study at 550 nm	Previous study	Present study at 550 nm	Previous study
Delhi	0.75 ± 0.05		0.86 ± 0.01	0.79 ± 0.05[a]	0. 9± 0.05		0.82 ± 0.06		0.84 ± 0.07	
Kanpur	0.75 ± 0.04	0.89[b]	0.86 ± 0.01	0.87 ± 0.019[c]	0.9 ± 0.01	0.89[d]	0.88 ± 0.03	0.9[d]	0.85 ± 0.06	0.88–0.92[e]
Ahmedabad	0.81 ± 0.04		0.9 ± 0.03	0.84 ± 0.04[f]	0.96 ± 0.01		0.93± 0.04		0.90 ± 0.07	
Gadanki	0.89 ± 0.01		0.89 ± 0.02		0.97 ± 0.005		0.93 ± 0.02		0.92 ± 0.04	0.92–0.99[g]
Jaipur	0.82 ± 0.04		0.92 ± 0.02	0.88 ± 0.023[c]	0.94± 0.02		0.83 ± 0.03		0.89 ± 0.06	
Gandi College	0.77 ± 0.04		0.85 ± 0.02	0.88 ± 0.028[c]	0.90± 0.02		0.79 ± 0.04		0.84 ± 0.06	

[a] *Panditharai et al.* [2008].
[b] *Singh et al.* [2004] at 440 nm.
[c] *Gautam et al.*,[2011]at 441 nm.
[d] *Dey and Tripathi* [2008].
[e] *Jethva et al.* [2005] at 441 nm.
[f] *Ganguly et al.* [2005].
[g] *Gadhavi and Jayaraman* [2010].

the SW monsoon season (i.e., June-September; Figure 3), as reported in previous studies [*Dash et al*., 2009]. The major rainfall belt associated with the Indian summer monsoon, including the belt extending from west-northwestward across the IGP to the head of Bay of Bengal, the equatorial Indian Ocean belt, and the belt at the western Ghats along the west coast of the peninsula [*Gadgil and Sajani*, 1998] is broadly well simulated, while the orographic rainfall belt near the northern IGP is lacking (Figure 3). The model is able to reproduce high rainfall events over the north-east Himalayas during the SW monsoon season. In addition, the model is also able to capture the coastal (west and east) precipitation, but it underestimates the inland precipitation, especially over the south Indian regions, compared to IMD observations (Figure 3). There are discrepancies between the spatial distribution of rainfall simulated by the model and the observations (mean bias = −2.7), especially over northern India and the NWI region, during the SW monsoon season. This is likely due to the simulation of too low orographic rainfall over the northern Indian region (Figure 3). In GCMs, the simulation of precipitation, especially high precipitation events, relies on parameterizations, such as cumulus convection and large-scale condensation. Thus, in general, inaccuracies could arise in precipitation magnitudes simulated by atmospheric GCMs [*Gadgil and Sajani*, 1998], even though large-scale monsoon features are preserved in ECHAM [*Annamalai et al*., 2007]. However, the interseasonal variability is clearly visible in the model-simulated rainfall distribution over the Indian region (Figure 3).

[26] Zonal-mean rainfall (mm/day) is simulated reasonably well in two different seasons (NE monsoon (bias = −0.07), and inter-monsoon (bias = −0.3) season) and broadly (bias = −0.7) during pre-monsoon season (Figure S3). Convective rainfall was found to be dominant over south and central Indian regions, while large-scale precipitation dominates over the northern Indian regions (Figure S3). It is known that a significant fraction (65%–75%) of total precipitation in the models originates from convective events rather than stratiform events in the tropics [*Dai*, 2001; *Tost et al*., 2006]. TRMM retrievals in the South Asian summer monsoon suggest that 46% of the precipitation stems from stratiform clouds and 44% from convective clouds, with the remaining 10% classified as neither stratiform nor convective in the observations [*Romatschke and Houze*, 2011]. The model-simulated zonal-mean rainfall shows that rainfall in the western regions (low total precipitation) is almost exclusively convective, while rainfall in the eastern Himalayan (higher total precipitation) is heavily stratiform during the SW monsoon season (Figure S3), which is consistent with findings from TRMM data over South Asian region [*Romatschke and Houze*, 2011]. During the SW monsoon season, the magnitude of zonal-mean rainfall was not predicted accurately; the rainfall values are underestimated by a factor of 2–3 (Figure S3). In the SW monsoon season, high rainfall was found over the CNI and NEI regions (Figure 3). Model-simulated zonal-mean rainfall is especially underestimated (by a factor of 2–3) over the latitudinal band of 19°N–25°N, where the model shows about equal contributions by both convective and large-scale rainfall values (Figure S3). The magnitude of model-simulated zonal-mean rainfall, on the other hand, agrees much better with observations (both in situ and satellite) over

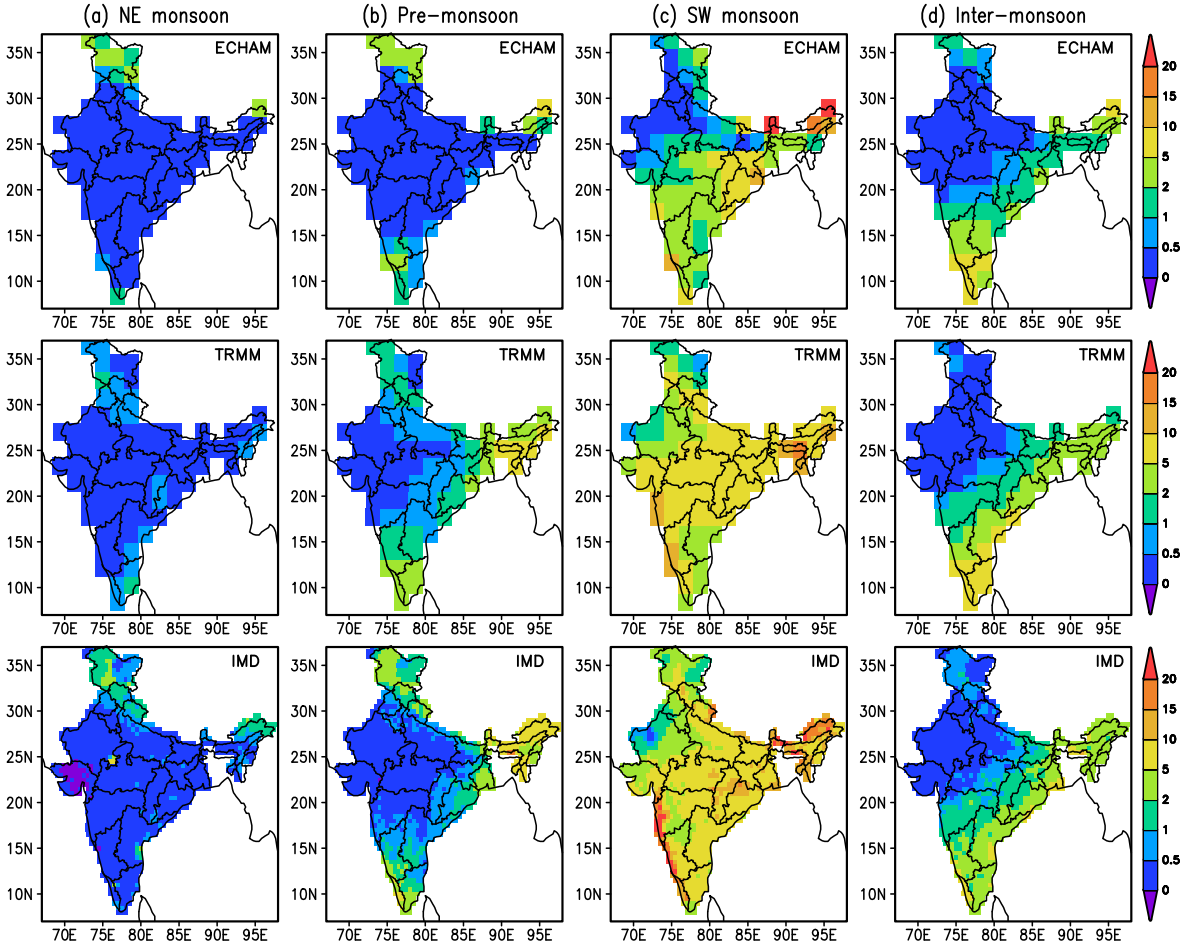

Figure 3. Seasonal-mean distribution of the model-simulated total precipitation (mm/day) for the nudged present-day simulation compared to TRMM (0.25° × 0.25°) satellite-retrieved rainfall and IMD (0.5° × 0.5°) rain gauge rainfall observations over the Indian region (January 2001 to December 2005).

the latitudinal band of 27°N–30°N, which is dominated by large-scale precipitation. The high rainfall over these latitudinal belts, particularly over the Himalayan foothills, is attributed to orography. It is known that TRMM captures the pattern of orographic rain seen in the IMD data but consistently underestimates the rainfall amounts, which is consistent with our findings (Figure S3). In summary, the model broadly captures the observed seasonal rainfall variability both in magnitude and spatial distributions over the Indian region during the 2001–2005 period, with some underestimation in absolute values, in particular in summer (SW monsoon season).

[27] We find that we may have confidence in the simulation of the spatiotemporal variability of model AOD and precipitation, but with some caution on the absolute values. For the subsequent analysis of the anthropogenic contribution, this implies that spatial patterns of signals may be more reliable than the absolute magnitudes.

4.2. Anthropogenic Aerosol Emissions Induced Variability

[28] In this section, the sensitivity of the climate response over the Indian subcontinent to anthropogenic aerosol emissions is evaluated and discussed. In the following analysis, we focus on the differences between the experiment with the PD and PI anthropogenic aerosol emissions, averaged for 5 years for the period from January 2001 to December 2005 (i.e., $\Delta = PD - PI$).

4.2.1. Aerosol Optical Depth

[29] A statistically significant (95% confidence level) change (PD-PI) of the order of 10–20% in seasonal-mean AOD was found from the enhanced anthropogenic emissions over the Indian subcontinent in all four seasons (Figure 4). The model-simulated AOD values increased by about 0.1–0.25 (in absolute values) during the biomass burning season (NE monsoon) over the IGP, CNI, and south India regions (Figure 4). In the pre-monsoon season, the highest changes in AOD (0.15–0.2) are found over the highly populated and industrialized regions (IGP and CNI), and extending over the east coast into the continent, with a marked northwest-southeast gradient. In the SW monsoon season, the largest changes in AOD (>0.2) are found over CNI and some parts of the IGP regions. A similar increase in AOD is simulated over the IGP and NWI regions during the inter-monsoon season (Figure 4). Somewhat smaller changes are found in the NE monsoon and pre-monsoon season than in SW monsoon season over the CNI region (Figure 4). This is due to the contribution of water soluble aerosols (sulfate) through aerosol hygroscopic growth over these regions.

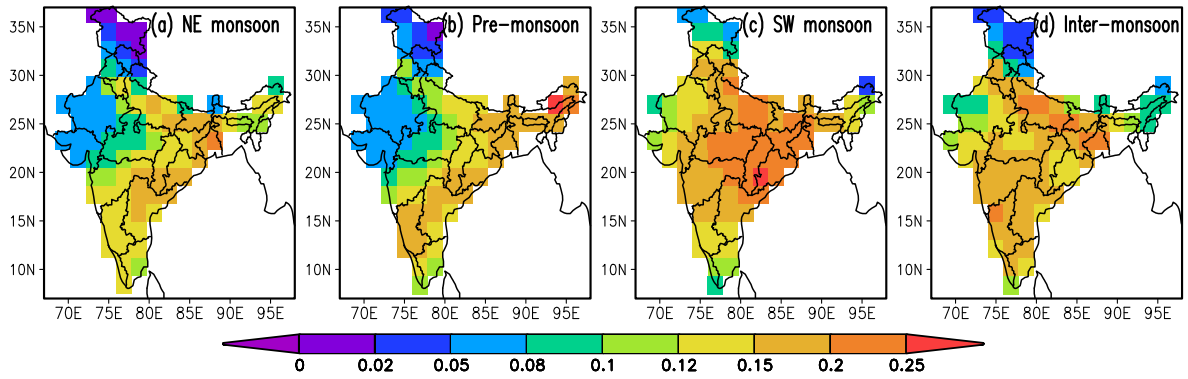

Figure 4. Model-simulated anthropogenic aerosol-induced change (PD-PI) in seasonal-mean AOD at 550 nm over the Indian subcontinent (January 2001 to December 2005).

[30] Based on MODIS retrievals, recent studies found increasing AOD trends (>10%) over the southern and central parts of the Indian subcontinent [*Alpert et al*., 2012]. Because of the mixing of aerosols by natural and anthropogenic sources, satellite measurements cannot distinguish whether these trends resulted from changes in natural or anthropogenic aerosols. However, assuming that, on average, long-term changes in natural aerosols are relatively small compared to those in anthropogenic aerosols, the observed increasing trends may be attributed to changes in anthropogenic aerosols [*Alpert et al*., 2012]. It should be emphasized that these trends are derived from very short time scales and highly uncertain.

4.2.2. Aerosol Direct Radiative Forcing

[31] The changes in model-simulated clear-sky short-wave radiation fluxes are analyzed at the top of the atmosphere (TOA), at the surface (SUR), and within the atmosphere (ATM) to quantify the seasonal differences in the anthropogenic aerosol-induced changes in atmospheric heating and surface cooling patterns over the Indian subcontinent (Figure 5). The changes (PD-PI) in clear-sky direct aerosol forcing at the TOA ranges from −0.17 (pre-monsoon) to −0.92 W m^{-2} (inter-monsoon) over the Indian subcontinent (Table 3). The increase in clear-sky atmospheric absorption (by up to 6–9 W m^{-2} in the seasonal-mean) can be attributed mainly to the enhanced absorption aerosol optical depth over the Indian region (Figure 2 and Figure S4). The seasonal-mean clear-sky radiative forcing at the surface shows a significant cooling (−6.9 to −9.9 W m^{-2}) over the Indian region (Table 3). The changes in the clear-sky solar radiation at the surface are to a large extent the mirror image of the changes in absorption within the atmosphere, rather than increased sunlight reflection at the TOA, similar to the results of previous studies [*Roeckner et al*., 2006]. Statistically significant regional changes in atmospheric forcing are simulated for the NWI (4.7 to 9.1 W m^{-2}), CNI (6.8 to 10.3 W m^{-2}), and NEI (5.4–12.8 W m^{-2}) regions because of enhanced BC aerosols (Figure 2) mainly arising from biofuel burning, crop-residue burning, and forest burning sectors. *Venkataraman et al*. [2006] show that BC aerosols are mainly (>80%) produced from the biofuel, forest, and crop-residue burning emission sectors over these regions.

[32] High surface cooling effects (−11.2 to −16.5 W m^{-2}) are simulated over the high anthropogenic emission source regions (IGP) over the Indian subcontinent during all seasons (Figure 5). This solar dimming effect of anthropogenic aerosols through atmospheric extinction leads to strong surface cooling and atmospheric warming over the high aerosol loading regions (IGP and CNI). The perturbation in radiation fluxes by the anthropogenic aerosol thus affects the stability of the troposphere over these regions (see section 4.2.4). The changes in clear-sky surface dimming which result from PD anthropogenic emissions, locally exceed −7 W m^{-2}. *Padma Kumari and Gosw*ami [2010] report observed trends in clear-sky solar dimming of −6 W m^{-2}/decade, averaged over 12 stations, occurred during 1981–2006. The emission data of SO_2 for the Indian region of *Lamarque et al*. [2010] show three quarters of increase in emissions from PI to PD during the 1981–2005 period. Thus, the results of *Padma Kumari and Goswami* [2010] correspond to a PD-PI difference of approximately −11 W m^{-2}, which is close to our model results. These trends are, in general, broadly comparable with the reported clear-sky solar dimming over the Indian region [*Soni et al*., 2012] and with the regional solar radiation trends estimated from Modern Era Retrospective-analysis for Research and Applications (MERRA) data presented by *Urankar et al*. [2012]. The surface cooling effect shows a maximum during the NE monsoon season. While inter-monsoon season precedes the atmospheric warming peak over the entire north Indian region, except in the NEI region (Figures 5e and 5f). This is because the winter has a more stable boundary layer and thus enables the surface to respond more to surface forcing than in pre-monsoon and monsoon season when the surface is climatologically warmer (Figure 5c) and boundary layer mixing is more deeper and active [*Chung and Ramanathan*, 2004]. It is also known that absorbing carbonaceous aerosols are mostly confined within the shallow boundary layer in the inter-monsoon and NE monsoon seasons over the Indian subcontinent [*Tripathi et al*., 2005]. The short-wave clear-sky aerosol radiative forcing from enhanced anthropogenic aerosol emissions between PI and PD levels over the Indian region is substantial. The main contributor to atmospheric aerosol absorption is BC emissions, which have increased by a factor of 8 over the Indian region (Figure S5a). The emissions of anthropogenic SO_2, the precursor gas to the scattering sulfate aerosols, increased by a factor of 10, while the emissions of OC have had a smaller increase with a factor of 2–3 (Figures S5b and S5c). The PD OC emissions show gradual

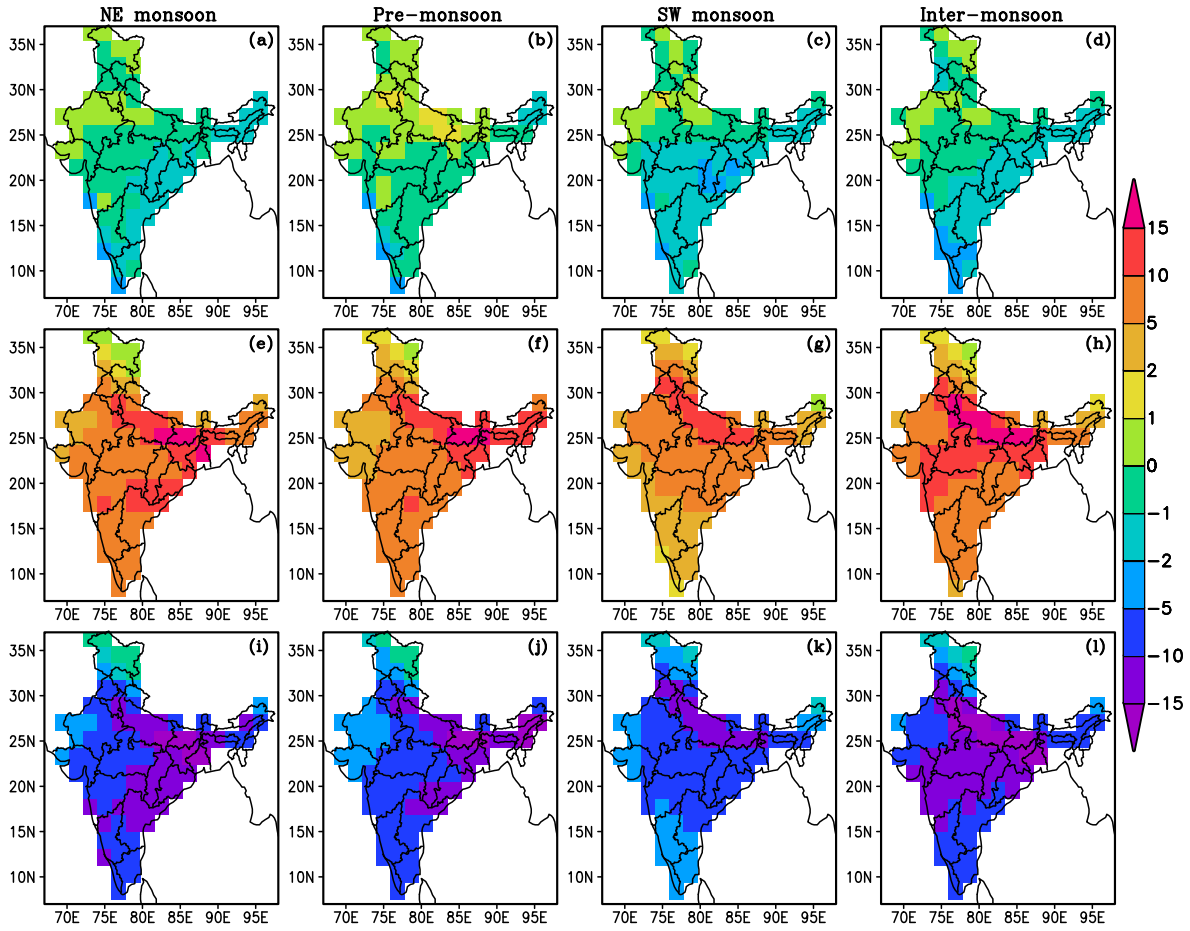

Figure 5. Spatial distribution of the model-simulated seasonal-mean change (PD-PI) in short-wave clear-sky aerosol radiative forcing (ARF, W m^{-2}) due to anthropogenic aerosol over the Indian subcontinent (January 2001 to December 2005), (a–d) at the top of the atmosphere, (i–l) at the surface, and (e–h) due to absorption within the atmosphere. The forcing is computed as the difference in mean radiative fluxes between the simulations with present-day (PD) and pre-industrial (PI) anthropogenic aerosol emissions.

Table 3. Season Mean Anthropogenic Aerosol-Induced Variability (PD-PI) in Clear-Sky Short-Wave Aerosol Direct Radiative Forcing (W m^{3-2}) at the Top of the Atmosphere (TOA), Surface (SUR), and Within the Atmosphere (ATM)

Region	NE Monsoon	Pre-Monsoon	SW Monsoon	Inter-Monsoon
India				
TOA (Wm^{-2})	−0.70	−0.17	−0.88	−0.92
ATM (Wm^{-2})	8.21	8.09	6.07	9.02
SUR (Wm^{-2})	−8.91	−8.26	−6.95	−9.94
CNI				
TOA (Wm^{-2})	−0.98	−0.31	−1.69	−1.05
ATM (Wm^{-2})	10.13	9.17	6.82	10.36
SUR (Wm^{-2})	−11.11	−9.48	−8.52	−11.42
IGP				
TOA (Wm^{-2})	−0.18	0.68	−0.23	−0.25
ATM (Wm^{-2})	13.32	11.94	10.99	16.25
SUR (Wm^{-2})	−13.5	−11.26	−11.22	−16.5
NWI				
TOA (Wm^{-2})	−0.13	0.17	−0.51	−0.26
ATM (Wm^{-2})	7.18	4.77	5.18	9.15
SUR (Wm^{-2})	−7.31	−4.6	−5.69	−9.41
NEI				
TOA (Wm^{-2})	−1.01	−0.69	−1.02	−1.41
ATM (Wm^{-2})	7.48	12.84	5.43	6.61
SUR (Wm^{-2})	−8.49	−13.53	−6.45	−8.02

increase from 15°N and peaks over the Himalayan region (29°N–30°N), while BC emissions show two peaks one around 10°N and other one around 30°N. A consequence of the stronger increase in BC is an enhanced atmospheric heating in different seasons over the Indian region.

4.2.3. Aerosol Indirect Effects

[33] Aerosol indirect radiative effects, defined here as cloudy-sky change in radiative fluxes (see section 3), are now examined to understand the indirect aerosol effects on the radiation budget resulting from the PD anthropogenic aerosol emissions. It is found that the indirect radiative effects both at the TOA and the surface are up to −8 W m^{-2} over the CNI regions in both nudged and the ensemble mean of the non-nudged simulations, but much smaller otherwise, and with only negligible absorption within the atmosphere (Figure 6). This reflects the total aerosol indirect effects, by which increased concentrations of cloud condensation nuclei (CCN) result in increased concentrations of cloud droplets, and subsequently an enhancement in cloud albedo [*Twomey*, 1977]. It is known that aerosol indirect forcing over Indian region during summer monsoon can range from −4.2 to −14 W m^{-2} [*Pandithurai et al.*, 2012].

[34] Interestingly, the indirect radiative effects at the TOA exhibit statistically significant, quite different, trends between

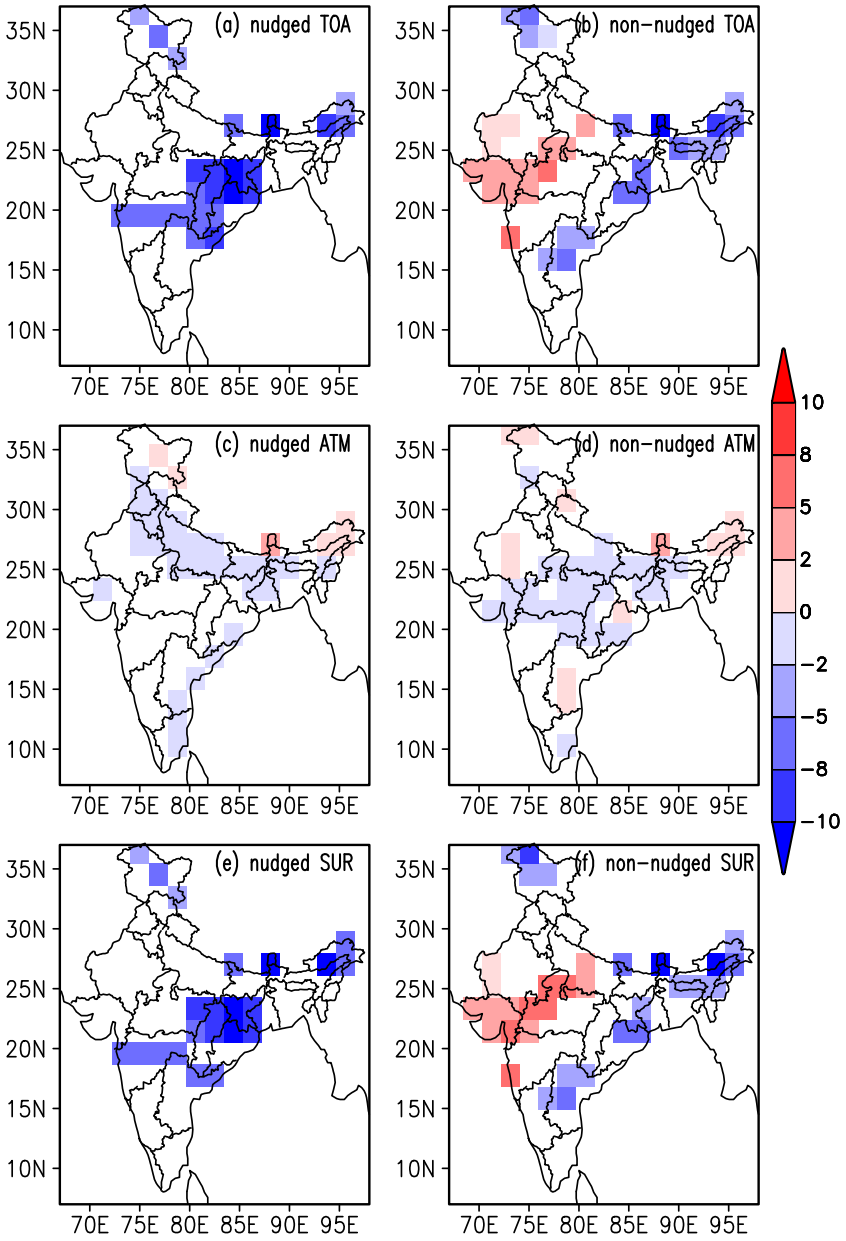

Figure 6. Spatial distribution of model-simulated seasonal-mean change (PD-PI) in short-wave cloudy-sky forcing (W m^{-2}) at the (a and b) top of the atmosphere (TOA), (e and f) surface (SUR), and (c and d) within the atmosphere (ATM) due to the present-day anthropogenic aerosol emissions over the Indian subcontinent during the SW monsoon period (January 2001 to December 2005). Only statistically significant differences (95% confidence according to a *t* test) are shown. The left column shows the nudged simulations (Figures 6a, 6c, and 6e), while the right column shows the ensemble mean of the three non-nudged simulations (Figures 6b, 6d, and 6f).

the nudged and non-nudged simulations (Figures 6a and 6b). In the non-nudged simulation, indirect radiative effect shows positive statistically significant flux differences in the NWI region, while in the east-coast area, there are negative fluxes. This feature is replaced by a large negative flux area, but no positive statistically significant flux, in the nudged simulation. This indicates that such a dipole feature is very sensitive to the perturbations to the large-scale atmospheric circulation features, which are constrained in the nudged simulation.

[35] However, changes (PD-PI) in the long-wave (LW) absorption from tropospheric anthropogenic aerosols arising from CCN are found to be very small compared to the short-wave component and not statistically significant (not shown). This is consistent with the findings from previous studies [*Stier et al.*, 2007]. The LW cloudy-sky radiative forcing, which was closely connected to high clouds, shows much smaller differences between PI and PD.

4.2.4. Precipitation

[36] The seasonal-mean change (PD-PI) in total precipitation is negative over most of the Indian subcontinent, but generally small (−0.5 to −1.5 mm d^{-1}). Precipitation changes are found to be statistically significant (95% confidence level

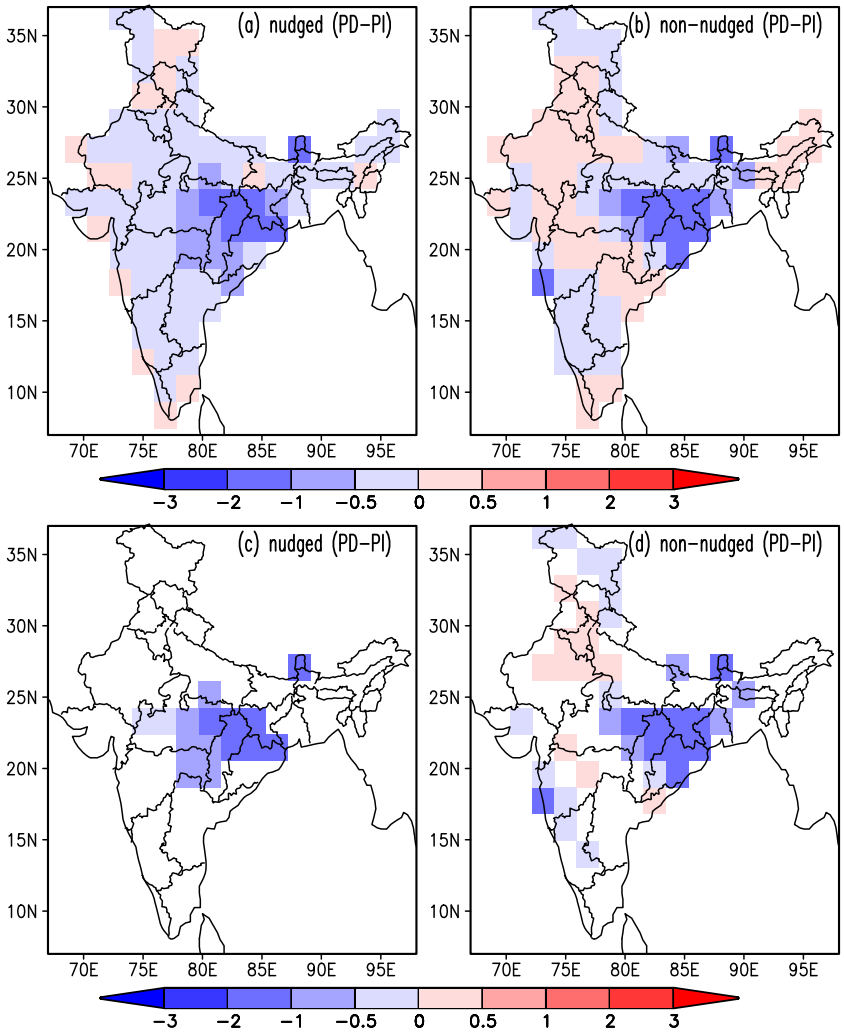

Figure 7. Spatial distributions of model-simulated seasonal-mean change (PD-PI) in total precipitation (mm/day) due to anthropogenic aerosol emissions over the Indian subcontinent during the SW monsoon period (2001 to 2005). The left column shows the nudged simulations (Figure 7a), while the right column shows the ensemble mean of the three non-nudged simulations (Figure 7b). Only regions where the differences (PD-PI) are statistically significant at the 95% confidence level were shaded in the bottom panel (Figures 7c and 7d). Only the SW monsoon season is shown because changes in the other seasons are not found to be statistically significant at the 95% confidence level anywhere on the continent.

based on a Student's *t* test analysis) only for SW monsoon season, and only over the CNI region (Figure 7). Only the SW monsoon season changes (PD-PI) in precipitation are discussed here because these changes in the other three seasons are not found to be statistically significant at the 95% confidence level anywhere on the continent. The decrease in SW monsoon rainfall over the CNI corresponds well to the observed rainfall trends from 1951 to 2003 by *Ghosh et al*. [2009]. However, some of the finer regional features seen in the observed rainfall trends are not captured in the model which may be due to low model horizontal resolution (180 km). Also, because of the model setup, changes near the coasts in the simulation are limited since the prescribed SST boundary conditions remain the same in both PD and PI simulations.

[37] To understand the influence of temporal changes in aerosol forcing on precipitation (influence of selection of seasons on the conclusions), the rainfall trends are examined during bi-monthly averaged periods. The analysis is carried out now in six periods: (1) January-February, (2) March-April, (3) May-June, (4) July-August, (5) September-October, and (6) November-December. The nudged experiments are used for this analysis. A statistically significant decreasing precipitation change is found only during the July-August period (region inside the black square indicates the statistically significant changes at 95% confidence interval; Figure S6d). It indicates that a 2 month average precipitation also captures most of the statistically significant precipitation trend observed during seasonal-mean (JJAS) analysis over the CNI region. However, seasonal analysis improves the statistical significance of the simulated precipitation trends over the CNI region during the SW monsoon season (Figure 7). Rainfall trend studies using seasonal (JJAS) mean have showed that the monsoon rainfall has weakened or decreased in the last 50 years over the central-north India region [*Dash et al*., 2009; *Ghosh*

et al., 2009; *Lau and Kim*, 2010]. Parsing precipitation trends into bi-monthly periods allowed identification of separate positive trends (increase) in May-June in the north-western regions and negative trends (decrease) in the central and southern regions, which is consistent with the findings from previous studies [*Lau and Kim*, 2010].

[38] In the nudged simulations, the large-scale meteorology was constrained toward re-analysis data. It is thus interesting to further investigate whether additional changes occur if the model is free to run in climatological mode with prescribed SST and SIC. For understanding the atmospheric circulation impacts on anthropogenic aerosol-induced precipitation changes, ensemble mean of the three non-nudged simulations is used. These free simulations also show a statistically significant (at the 95% confidence level) decreasing precipitation trend over the CNI region (Figure 7), but of larger intensity, and with a broader geographical extent. In addition, small increasing trends are found over the north-western part of the IGP region in the free simulations. This slight increase in precipitation is consistent with the trends analysis in the observed rainfall during 1951–2003 by *Ghosh et al*. [2009]. The anthropogenic aerosol-induced changes on monsoon precipitation are more prominent in the non-nudged simulations compared to that from the nudged simulations. Such a slight difference in results is expected due to the difference in the large-scale atmospheric dynamics between the two simulations. However, this difference in the response of precipitation between the nudged and non-nudged simulations is only small, which is similar to the findings from previous studies [*Lohmann and Hoose*, 2009]. To examine the decreasing trend of total precipitation further, the convective and large-scale precipitation anomalies (PD-PI) were analyzed separately during the SW monsoon period. The model shows that changes in convective precipitation drive the decreasing trend in total precipitation (Figure 8). The stratiform precipitation shows statistically insignificant trends (not shown) over the Indian region during this period.

[39] The "cloud lifetime effect" on stratiform clouds is associated with a higher amount of cloud water from increased anthropogenic aerosol emissions. This is because an increase in anthropogenic aerosol concentration leads to the formation of large amount of smaller-sized super-cooled cloud droplets that reduce the formation of rain drops and enhance the residence time of cloud water [*Lohmann and Feichter*, 1997]. This effect is parameterized in the GCM and leads to the enhancement of cloud water in the CNI region (Figure 9a and 9e). It was found that the increase in anthropogenic aerosol emissions since the beginning of the industrialization has caused a reduction in solar radiation at the surface (solar dimming) and a decrease in precipitation in the tropical regions, particularly in regions with large aerosol loads [*Feichter et al*., 2004; *Roeckner et al*., 2006].

[40] To examine further the forcing mechanisms leading to the surface cooling, the influence of enhanced anthropogenic aerosol emissions on stratiform cloud droplet number concentration (CDNC) burden (m^{-2}) is analyzed during the SW monsoon (Figure 10). This is computed as the difference between PD and PI simulations, and positive values, as shown in red, correspond to the expected increase in CDNC with enhanced anthropogenic aerosol emissions (Figure 10). A thorough evaluation of the cloud microphysics scheme used in the ECHAM5-HAM model was carried out by *Lohmann et al*. [2007] who found that the simulated column CDNC agrees well with satellite retrievals. Here, a large increase in CDNC was found over CNI region, which mainly results from the large increase in sulfate aerosols. Increase in CDNC then further leads to less coalescence efficiency in the model simulation (parameterized using the autoconversion formulation of *Khairoutdinov and Kogan* [2000]) and thereby increasing cloud lifetime and hence increased surface aerosol indirect forcing over the CNI region.

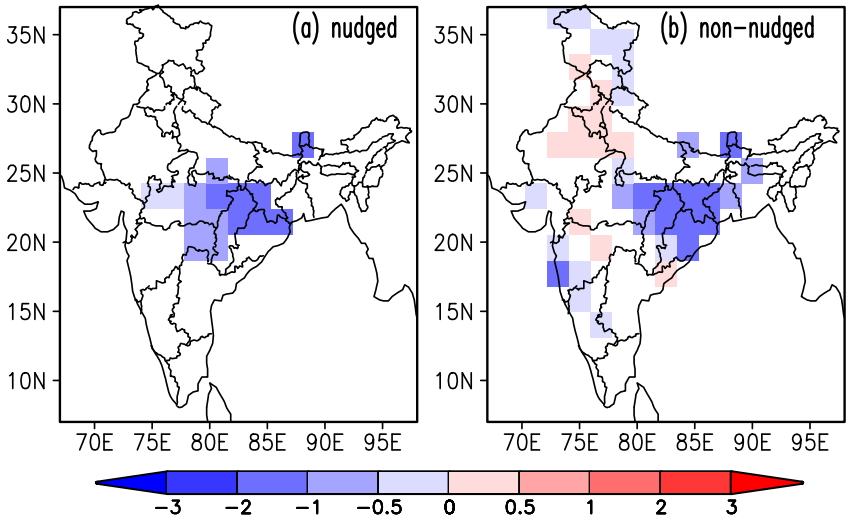

Figure 8. Spatial distributions of model-simulated seasonal-mean change (PD-PI) in convective precipitation (mm/day) due to anthropogenic aerosol emissions over the Indian subcontinent during the SW monsoon period (2001–2005). The left column shows the nudged simulations (Figure 8a), while the right column shows the ensemble mean of the three non-nudged simulations (Figure 8b). Only regions where the differences (PD-PI) are statistically significant at the 95% confidence level were shaded.

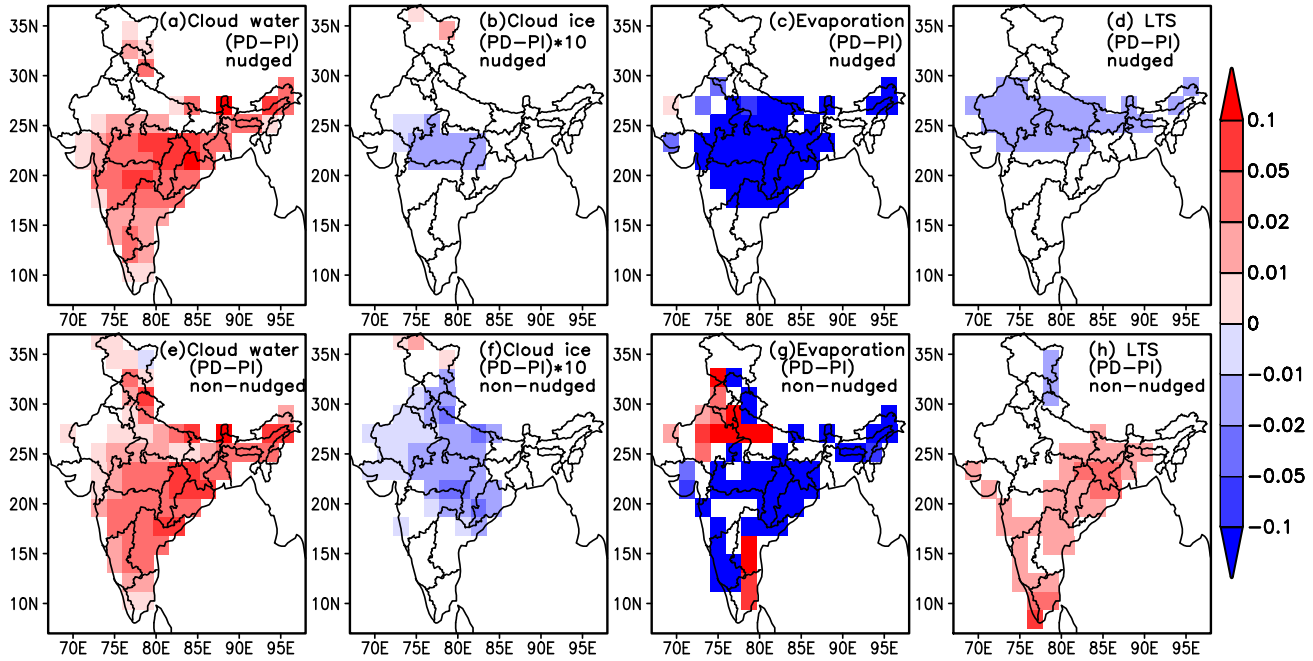

Figure 9. Spatial distributions of model-simulated SW monsoon seasonal-mean change (PD-PI) due to anthropogenic aerosol emissions for vertically integrated cloud water ($g\,m^{-2}$, 9a and 9e), vertically integrated cloud ice ($g\,m^{-2}$, 9b, and 9f), evaporation ($kg\,m^{-2}\,day^{-1}$, 9c and 9g) and lower tropospheric stability (LTS, 9d and 9h) and lower tropospheric stability (LTS, 9d and 9h) during the SW monsoon period (2001–2005). Only regions where the differences (PD-PI) are statistically significant at the 95% confidence level were shaded. The top panel shows the nudged simulations, while the bottom panel shows the ensemble mean of the three non-nudged simulations.

[41] In the simulations, a strong radiative cooling of the surface is simulated over much of the Indian subcontinent resulting from the direct aerosol effect. For the indirect effect, in the nudged simulation, the surface cooling is particularly strong over the CNI region, where a decreasing precipitation trend is found. These surface cooling effects

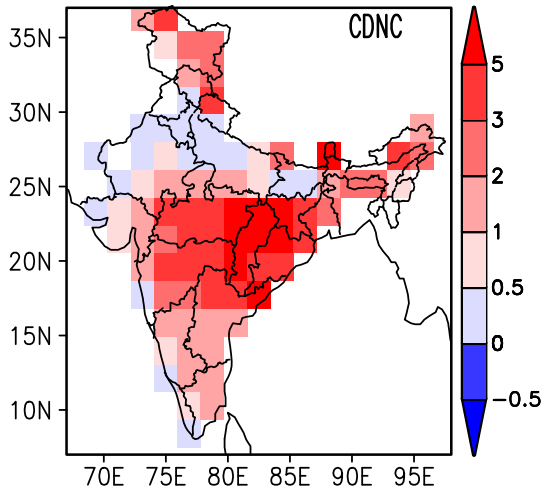

Figure 10. Spatial distributions of model-simulated seasonal-mean statistically significant (95%) anthropogenic aerosol-induced change (PD-PI) in cloud droplet number concentration (CDNC) burden (m^{-2}), multiplied by 1×10^{-10} for the nudged simulation over the Indian subcontinent during the SW monsoon period (2001–2005).

(solar dimming) in the simulation may thus be considered the main drivers of the reduction in precipitation. It is worth noting that the "cloud lifetime effect" does not directly reduce accumulated precipitation, but rather adds to the effect via radiation. In the simulations, this is manifested in the result that the reduction in total precipitation is mostly from the reduction in convective precipitation which is not directly affected by the cloud lifetime effect in the model, but rather influenced via changes in radiation.

[42] Surface evaporation rate ($kg\,m^{-2}\,d^{-1}$) anomalies (PD-PI) were found to be negative during the SW monsoon period due to enhanced anthropogenic aerosol emissions and subsequently reduced surface solar radiation (Figures 9c and 9g). Decreases in surface evaporation (0.05–0.15) were found in regions (CNI region) where the maximum changes in AOD are simulated during the SW monsoon season (Figures 9c and 9g). At the surface, there is a balance between radiation, evaporation (latent heat flux from the surface to the atmosphere), sensible heat flux, and heat conduction into the solid Earth. One or all of these components will decrease to compensate for the reduction in surface solar radiation. The absorbed solar radiation at the surface was mainly balanced by evaporation, and it is thus concluded that a major fraction of the reduction in surface solar radiation (Figure 5) is balanced by a reduction in evaporation. This reduction then leads to a reduction in convection and convective rainfall and effectively locally spins down the hydrological cycle. As evaporation change has to balance with precipitation on a global scale, a reduction in evaporation (latent heat flux) leads to a reduction in rainfall over the CNI region. However, an increase in evaporation in the non-nudged simulation

(Figure 9g) leads to an increase in precipitation over the north-western part of the IGP region (Figures 7 and 8). Cloud ice content ($g\,m^{-2}$) was also found to be slightly decreased over CNI region (Figures 9b and 9f). This is likely due to the reduced convective activity and the reduced transport of water to the upper atmosphere.

[43] In order to better understand the causes for the precipitation reduction simulated in the GCM, and in particular the stronger reduction in the free simulation, where the indirect forcing is found to be a less clear driver of the precipitation effect, we analyze the seasonal-mean lower tropospheric stability ($LTS = \theta_{700hPa} - \theta_{sfc}$), which is defined as the difference in potential temperature (θ) between the 700 hPa level and the surface [*Klein and Hartmann*, 1993; *Medeiros and Stevens*, 2011] anomalies (PD-PI; Figure 9d and 9h). In the nudged simulations, very small, statistically insignificant changes (PD-PI) are found in LTS (i.e., temperature at surface and 700 hPa levels) over the CNI region. The small LTS change found in the nudged simulations is expected since temperatures are constrained (Figure 9d). In the nudged simulation, a reduction in evaporation leads to a rainfall reduction over the CNI region. In contrast, in the free simulation, a stabilization of the lower troposphere is simulated over the CNI region (Figure 9h). This stabilization in the non-nudged simulations can be attributed to the less solar radiation in the boundary layer due to enhanced CDNC and cloud liquid water (Figure 9e), and the simultaneous cooling of the surface by atmospheric extinction because of the enhanced PD anthropogenic aerosol emissions (Figure 5). This stabilization is the reason for the slightly higher precipitation reduction in the free simulations compared to that in nudged simulations, despite the pattern being slightly different from the precipitation change pattern. Here, as a cautionary note, we would like to point out that the inclusion of cloud layer in the LTS calculations may have some influence on the simulated changes in the stability during cloudy-sky days.

[44] Recent modeling studies found that absorbing aerosol (BC) forcing tends to overcome the stabilizing effect resulting in increased precipitation in the early part of SW monsoon season [*Menon et al*., 2002; *Lau et al*., 2006; *Randles and Ramaswamy*, 2008]. In these studies the aerosols were prescribed, based on off-line calculations, for estimating the radiative forcing using the model radiation code and then used to understand the climate response. This approach has been used widely but is not guaranteed to generate an accurate aerosol radiative forcing because it does not account for potential feedbacks—in particular, wet scavenging of aerosol by precipitation—between the forcing and the response. *Meehl et al*. [2008] also found that BC aerosol forcing increased the precipitation during the pre-monsoon season and produced decreased rainfall during the monsoon season over India in their model. In our study, an interactive online aerosol module with more complex and more realistic aerosol microphysics [*Stier et al*., 2005] and a two-moment cloud microphysics scheme on stratiform clouds [*Lohmann et al*., 2007] are used to examine the local anthropogenic aerosol forcing response on monsoon precipitation. Therefore, we believe that our findings, which are in part contrary to earlier findings based on absorbing aerosols, are more realistic because they account for the aerosol mixing and its influence on atmospheric extinction (both scattering and absorption) as well as accounting for the potential feedbacks between the forcing and the response. Our findings with regard to the response of convective precipitation to anthropogenic aerosols are broadly consistent with the findings from *Wang et al*. [2009], where both approaches used prognostic aerosol microphysics treatment for the analysis, while the aerosol indirect radiative effect and cloud microphysics treatment are different.

5. Conclusions

[45] Anthropogenic aerosol-induced changes in aerosol loading and their direct and indirect radiative effects on the south-west monsoon precipitation were examined over the Indian subcontinent during January 2001 to December 2005 using the ECHAM5.5-HAM model. In a first step, the model is evaluated using satellite retrievals. The model-simulated AOD at 550 nm broadly captures the spatial (distribution patterns) and temporal (interseasonal) variability over the Indian subcontinent. However, absolute magnitudes and some details of the variability are not well simulated. Similarly, both the spatial distribution and seasonal cycle of the simulated precipitation broadly capture the IMD-observed and TRMM satellite-retrieved distributions. In terms of absolute magnitude, the model underestimates precipitation particularly in the SW monsoon season. These findings imply that the characteristics of the AOD and precipitation change induced by anthropogenic aerosols may be simulated realistically, while the absolute magnitude of effects may still be somewhat questionable.

[46] The seasonal-mean anomalies (present-day(PD)-pre-industrial(PI)) in AOD and its climate effects were computed as the differences between an experiment with the PD anthropogenic aerosol emissions and an experiment with PI anthropogenic aerosol emissions, averaged for 5 years for the period from January 2001 to December 2005 (i.e., $\Delta = PD - PI$). The enhancement in PD anthropogenic aerosol emissions is reflected in the changes in total mid-visible (550 nm) AOD, including its seasonal variations particularly in the Indo-Gangetic Plain (IGP) and central-north India (CNI) regions. Increased anthropogenic activities lead to changes in biofuel emissions (domestic fuelwood and agriculture burning) and industrial emissions, leading to the seasonal enhancement in AOD values by about 0.1–0.25 (in absolute values) over India. The enhanced anthropogenic aerosol emissions reduced the solar flux to the surface (through atmospheric extinction, where absorption is more important than scattering, and through the "indirect effect" via cloud microphysics). The increase in CDNC, cloud liquid water, and cloud cover leads to less solar radiation in the boundary layer, which, in combination with the surface cooling, tends to stabilize the troposphere below the aerosol layer over the CNI region. The model simulates significant changes (PD-PI) in clear-sky surface net solar radiation (dimming by more than $-7\ W\,m^{-2}$), which agrees well with observed trends over the Indian region. This solar dimming effect of anthropogenic aerosols through atmospheric extinction leads to strong surface cooling and atmospheric warming over the high aerosol loading regions (over IGP and CNI). A statistically significant surface cooling effect (greater than $-10\ W\,m^{-2}$) is simulated by the model from enhanced PD anthropogenic aerosol emissions over the Indian subcontinent. The low-altitude surface cooling is caused primarily by the increase in the

BC absorption of solar radiation. Interestingly, the radiative effects during cloudy-sky conditions exhibit statistically significant, quite different, trends between the nudged and non-nudged simulations. This indicates that such features, especially at the TOA fluxes in the NWI region, are very sensitive to the perturbations to the large-scale atmospheric circulation features, which are constrained in the nudged simulation.

[47] Statistically significant decreasing surface precipitation from the enhanced anthropogenic aerosol emissions (PD-PI) is simulated only for the SW monsoon season over the CNI region. This simulated trend is consistent with observed rainfall trends since the mid-20th century. In the model, this decrease is dominated by a decrease in convective rather than stratiform precipitation. Similarity of spatial patterns suggests that the surface cooling forcing by mainly the aerosol indirect effect is responsible for this reduction in convective activity. When large-scale dynamics changes are allowed in an ensemble of non-nudged model simulations, the aerosol absorption in addition leads to a further stabilization of the lower troposphere, further reducing convective precipitation.

[48] The indirect aerosol effect generates surface cooling and lower solar radiation in the boundary layer due to enhanced stratiform CDNC, cloud liquid water, and cloud cover, which, together with atmospheric heating due to aerosol absorption, lead to an increase in lower tropospheric stability and subsequently to convective precipitation inhibition over the CNI region. Stronger surface cooling from aerosol indirect forcing along with direct aerosol forcing resulted in precipitation reduction over the CNI region during the SW monsoon season.

[49] Our study suggests that increased emissions of anthropogenic aerosols in PD cause a reduction in mean summer monsoon precipitation over the CNI region. Our analysis of the precipitation responses to aerosol radiative effects suggests that most of the precipitation reductions are caused by aerosol indirect aerosol effect, which generates surface cooling and lower solar radiation in the boundary layer due to enhanced stratiform CDNC, cloud liquid water, and cloud cover. Stronger surface cooling along with increased stability led to rainfall reduction over the CNI region. Our study, therefore, suggests that anthropogenic aerosols likely influence the hydrological cycle through significant cloud changes, increased stability, and reduced evaporation.

[50] Our study does not include a two-moment convective cloud microphysical scheme and related interactions with dynamical processes and precipitation. Early attempts to bring the two-moment microphysical scheme into convective parameterization of ECHAM5-HAM showed that increased CDNC led to a suppression of convective precipitation over the high aerosol loading regions (i.e., tropics) [*Lohmann*, 2008].

[51] In summary, the model simulates a widespread and substantial change in column aerosol concentration results from PD anthropogenic emissions, which lead to a widespread and strong surface cooling, consistent with observed trends. Significant cloud changes via indirect effects are confined to a smaller region in CNI, where a strong surface forcing is exerted in the SW monsoon season. A signal in precipitation is found only over CNI region, only in the SW monsoon season. This signal is consistent with observed trends. This precipitation reduction is from a reduction in convective precipitation. It is linked mainly to the surface cooling, and further substantially enhanced by the stability of the atmosphere through changes in CDNC, cloud water, and cloud cover.

[52] **Acknowledgments.** This work was supported through the Atmospheric Trace Gases-Chemistry, Transport, and Modeling (AT-CTM) project of the Indian Space Research Organisation's Geosphere Biosphere Programme (ISRO-GBP), Bengaluru, India. The satellite data used in this study are downloaded from GES-DISC, NASA. The rainfall data used in this study were acquired as part of the Tropical Rainfall Measuring Mission (TRMM). We acknowledge the Indian Meteorological Department (IMD) for providing the Indian rainfall gridded product. Computing time was provided by the German High Performance Computing Centre for Climate and Earth System Research (Deutsches Klimarechenzentrum, DKRZ). J. Quaas was supported by an Emmy Noether grant of the German Research Foundation (DFG). Ribu Cherian acknowledges the funding support from the Deutscher Akademischer Austausch Dienst (DAAD) for his visit to MPI-M (Hamburg, Germany). We acknowledge the constructive comments by Thara Prabha and two anonymous reviewers on an earlier version of this manuscript.

References

Alpert, P., O. Shvainshtein, and P. Kishcha (2012), AOD trends over megacities based on space monitoring using MODIS and MISR, *American Journal of Climate Change*, *1*, 117–131, doi:10.4236/ajcc.2012.13010.

Andreae, M. O., and D. Rosenfeld (2008), Aerosol-cloud-precipitation interactions. Part 1. The nature and sources of cloud-active aerosols, *Earth-Science Reviews*, *89*(1-2), 13–41.

Andreae, M. O., D. Rosenfeld, P. Artaxo, A. A. Costa, G. P. Frank, K. M. Longo, and M. A. F. Silva-Dias (2004), Smoking rain clouds over the Amazon, *Science*, *303*(5662), 1337–1342.

Andres, R. J., and A. D. Kasgnoc (1998), A time-averaged inventory of subaerial volcanic sulfur emissions, *J. Geophys. Res.*, *103*(D19), 25251–25261.

Annamalai, H., K. Hamilton, and K. R. Sperber (2007), The South Asian summer monsoon and its relationship with ENSO in the IPCC AR4 simulations, *J. Climate*, *20*(1071-1092), doi:10.1175/JCLI4035.1.

Bond, T. C., D. G. Streets, K. F. Yarber, S. M. Nelson, J. H. Woo, and Z. Klimont (2004), A technology-based global inventory of black and organic carbon emissions from combustion, *J. Geophys. Res.*, *109* (D14), doi:10.1029/2003JD003697.

Cherian, R., C. Venkataraman, S. Ramachandran, J. Quaas, and S. Kedia (2012), Examination of aerosol distributions and radiative effects over the Bay of Bengal and the Arabian Sea region during ICARB using satellite data and a general circulation model, *Atmos. Chem. Phys.*, *12*, 1287–1305, doi:10.5194/acp-12-1287-2012.

Chung, C. E., and V. Ramanathan (2004), Aerosol loading over the Indian Ocean and its possible impact on regional climate, *Indian Journal of Marine Sciences*, *33*, 40-55.

Cofala, J., M. Amann, and R. Mechler (2005), Scenarios of world anthropogenic emissions of air pollutants and methane up to 2030, International Institute for Applied Systems Analysis (IIASA)), Laxenburg, Austria.

Dai, A. (2001), Global precipitation and thunderstorm frequencies. Part I: Seasonal and interannual variations, *J. Climate*, *14*, 1092–1111.

Dash, S. K., M. A. Kulkarni, U. C. Mohanty, and K. Prasad (2009), Changes in the characteristics of rain events in India, *J. Geophys. Res.*, *114*, D10109, doi:10.1029/2008JD010572.

Dentener, F., et al. (2006), Emissions of primary aerosol and precursor gases in the years 2000 and 1750 prescribed data sets for AeroCom, *Atmos. Chem. Phys.*, *6*, 4321–4344.

Dey, S., and L. D. Girolamo (2010), A climatology of aerosol optical and microphysical properties over the Indian subcontinent from 9 years (2000–2008) of Multiangle Imaging Spectroradiometer (MISR) data, *J. Geophys. Res.*, *115*(D15204), doi:10.1029/2009JD013395.

Dey, S., and S. N. Tripathi (2008), Aerosol direct radiative effects over Kanpur in the Indo-Gangetic basin, northern India: Long-term (2001–2005) observations and implications to regional climate, *J. Geophys. Res.*, *113* (D04212), doi:10.1029/2007JD009029.

Dey, S., S. N. Tripathi, R. P. Singh, and B. N. Holben (2004), Influence of dust storms on aerosol optical properties over the Indo-Gangetic basin, *J. Geophys. Res.*, *109*(D20211), doi:10.1029/2004JD004924.

Di Girolamo, L., T. C. Bond, D. Bramer, D. J. Diner, F. Fettinger, R. A. Kahn, J. V. Martonchik, M. V. Ramana, V. Ramanathan, and P. J. Rasch (2004), Analysis of Multi-angle Imaging SpectroRadiometer (MISR) aerosol

optical depths over greater India during winter 2001–2004, *Geophys. Res. Lett.*, *31*(23), L23115, doi:10.1029/2004GL021273.
Feichter, J., E. Kjellstrom, H. Rodhe, F. Dentener, J. Lelieveld, and G. J. Roelofs (1996), Simulation of the tropospheric sulfur cycle in a global climate model, *Atmos. Environ.*, *30*(10-11), 1693–1707.
Feichter, J., E. Roeckner, U. Lohmann, and B. Liepert (2004), Nonlinear aspects of the climate change response to greenhouse gas and aerosol forcing, *J. Climate*, *17*, 2384–2398.
Forster, P., et al. (2007), Changes in atmospheric constituents and in radiative forcing, in Climate Change 2007: The Physical Science Basis-Contribution of Working Group I to the Fourth Assessment Report of the Intergovernmental Panel on Climate Change, edited by S. Solomon, D. Qin, M. Manning, Z. Chen, M. Marquis, K.B. Averyt, M. Tignor and H.L. Miller, pp. 153–171, Cambridge Univ. Press, Cambridge, U. K.
Gadgil, S., and S. Sajani (1998), Monsoon precipitation in the AMIP runs, *Climate Dynamics*, *14* (9), 659–689, doi:10.1007/s003820050248.
Gadhavi, H., and A. Jayaraman (2010), Absorbing aerosols: Contribution of biomass burning and implications for radiative forcing, *Ann. Geophys.*, *28*, 103–111, doi:10.5194/angeo-28-103-2010.
Ganguly, D., H. Gadhavi, A. Jayaraman, T. A. Rajesh, and A. Misra (2005), Single scattering albedo of aerosols over the central India: Implications for the regional aerosol radiative forcing, *Geophys. Res. Lett.*, *32* (L18803), doi:10.1029/2005GL023903.
Gautam, R., N. C. Hsu, K. M. Lau, S. C. Tsay, and M. Kafatos (2009), Enhanced pre-monsoon warming over the Himalayan-Gangetic region from 1979 to 2007, *Geophys. Res. Lett.*, *36*(L07704), doi:10.1029/2009GL037641.
Gautam, R., et al. (2011), Accumulation of aerosol over the Indo-Gangetic plains and southern slopes of the Himalayas: Distribution, properties and radiative effects during the 2009 pre-monsoon season, *Atmos. Chem. Phys.*, *11*, 12841–12863.
Ghosh, S., V. Luniya, and A. Gupta (2009), Trend analysis of Indian summer monsoon rainfall at different spatial scales, *Atmos. Sci. Lett.*, *10*(4), 285–290.
Goswami, B. N., V. Venugopal, D. Sengupta, M. S. Madhusoodanan, and P. K. Xavier (2006), Increasing trend of extreme rain events over India in a warming environment, *Science*, *314*, 1442–1445.
Hagemann, S., K. Arpe, and E. Roeckner (2006), Evaluation of the hydrological cycle in the ECHAM5 Model, *J. Climate*, *19*, 3810–3827.
Huffman, G. J., R. F. Adler, D. T. Bolvin, G. Gu, E. J. Nelkin, K. P. Bowman, Y. Hong, E. F. Stocker, and D. B. Wolff (2007), The TRMM Multi-satellite precipitation analysis: Quasi-global, multi-year, combined-sensor precipitation estimates at fine scale, *J. Hydrometeor*, *8*, 38–55.
Jethva, H., S. K. Satheesh, and J. Srinivasan (2005), Seasonal variability of aerosols over the Indo-Gangetic basin, *J. Geophys. Res.*, *110*, D21204, doi:10.1029/2005JD005938.
Jeuken, A. B. M., P. C. Siegmund, L. C. Heijboer, J. Feichter, and L. Bengtsson (1996), On the potential of assimilating meteorological analyses in a global climate model for the purpose of model validation, *J. Geophys. Res.*, *110*(D12), 16939–16950, doi:10.1029/96JD01218.
Khairoutdinov, M., and Y. Kogan (2000), A new cloud physics parameterization in a large-eddy simulation model of marine stratocumulus, *Mon. Wea. Rev.*, *128*, 229–243.
Kinne, S., et al. (2003), Monthly averages of aerosol properties: A global comparison among models, satellite data and AERONET ground data, *J. Geophys. Res.*, *108*(4634), doi:10.1029/2001JD001253.
Klein, S. A., and D. L. Hartmann (1993), The seasonal cycle of low stratiform clouds, *J. Climate*, *6*, 1587–1606.
Koffi, B., et al. (2012), Application of the CALIOP Layer Product to evaluate the vertical distribution of aerosols estimated by global models: Part 1. AeroCom phase I results, *J. Geophys. Res.*, *117*, D10201, doi:10.1029/2011JD016858.
Kripalani, R. H., J. H. Oh, A. Kulkarni, S. S. Sabade, and H. S. Chaudhari (2007), South Asian summer monsoon precipitation variability: Coupled climate model simulations and projections under IPCC AR4, *Theor. Appl. Climatol.*, *90*, 133–159, doi:10.1007/s00704-006-0282-0.
Kuhlmann, J., and J. Quaas (2010), How can aerosols affect the Asian summer monsoon? Assessment during three consecutive pre-monsoon seasons from CALIPSO satellite data, *Atmos. Chem. Phys.*, *10*, 4673–4688.
Lamarque, J.-F., et al. (2010), Historical (1850–2000) gridded anthropogenic and biomass burning emissions of reactive gases and aerosols: Methodology and application, *Atmos. Chem. Phys.*, *10*, 7017–7039, doi:10.5194/acp-10-7017-2010.
Lau, K. M., and K.-M. Kim (2010), Fingerprinting the impacts of absorbing aerosols on long-term trends of the Indian summer monsoon regional rainfall, *Geophys. Res. Lett.*, *37*(L16705), doi:10.1029/2010GL043255.
Lau, K. M., M. K. Kim, and K. M. Kim (2006), Asian summer monsoon anomalies induced by aerosol direct forcing: The role of the Tibetan Plateau, *Climate Dynamics*, *26*(7-8), 855–864.
Lohmann, U. (2008), Global anthropogenic aerosol effects on convective clouds in ECHAM5-HAM, *Atmos. Chem. Phys.*, *8*, 2115–2131.
Lohmann, U., and J. Feichter (1997), Impact of sulfate aerosols on albedo and lifetime of clouds: A sensitivity study with the ECHAM GCM, *J. Geophys. Res.*, *102*, 13685–13700.
Lohmann, U., and C. Hoose (2009), Sensitivity studies of different aerosol indirect effects in mixed-phase clouds, *Atmos. Chem. Phys.*, *9*, 8917–8934.
Lohmann, U., P. Spichtinger, S. Jess, T. Peter, and H. Smit (2008), Cirrus cloud formation and ice supersaturated regions in a global climate model, *Environ. Res. Lett.*, *3*, 045022.
Lohmann, U., P. Stier, C. Hoose, S. Ferrachat, S. Kloster, E. Roeckner, and J. Zhang (2007), Cloud microphysics and aerosol indirect effects in the global climate model ECHAM5-HAM, *Atmos. Chem. Phys.*, *7*, 3425–3446, doi:10.5194/acp-7-3425-2007.
Medeiros, B., and B. Stevens (2011), Revealing differences in GCM representations of low clouds, *Climate Dynamics*, *36*, 385–399.
Meehl, G. A., J. M. Arblaster, and W. D. Collins (2008), Effects of black carbon aerosols on the Indian monsoon, *J. Climate*, *21*, 2869–2882.
Menon, S., J. Hansen, L. Nazarenko, and Y. F. Luo (2002), Climate effects of black carbon aerosols in China and India, *Science*, *297*(5590), 2250–2253.
Nordeng, T. E. (1994), Extended versions of the convective parameterization scheme at ECMWF and their impact on the mean and transient activity of the model in the tropics, *Tech. Memo. Rep. 206*, 25 pp, European Centre for Medium-Range Weather Forecasts, Reading, United Kingdom.
Padma Kumari, B., and B. N. Goswami (2010), Seminal role of clouds on solar dimming over the Indian monsoon region, *Geophys. Res. Lett.*, *37*, L06703, doi:10.1029/2009GL042133.
Pandithurai, G., S. Dipu, K. K. Dani, S. Tiwari, D. S. Bisht, P. C. S. Devara, and R. T. Pinker (2008), Aerosol radiative forcing during dust events over New Delhi, India, *J. Geophys. Res.*, *113*(D13209), doi:10.1029/2008JD009804.
Pandithurai, G., S. Dipu, T. V. Prabha, R. S. Maheskumar, J. R. Kulkarni, and B. N. Goswami (2012), Aerosol effect on droplet spectral dispersion in warm continental cumuli, *J. Geophys. Res.*, *117*, D16202, doi:10.1029/2011JD016532.
Prabha, T. V., A. Karipot, D. Axisa, B. P. Kumari, R. S. Maheskumar, M. Konwar, J. R. Kulkarni, and B. N. Goswami (2012), Scale interactions near the foothills of Himalayas during CAIPEEX, *J. Geophys. Res.*, *117*, D10203, doi:10.1029/2011JD016754.
Rajeevan, M., J. Bhate, J. D. Kale, and B. Lal (2006), High resolution daily gridded rainfall data for the Indian region: Analysis of break and active monsoon spells, *Curr. Sci.*, *91*(3), 296–306.
Ramachandran, S., and R. Cherian (2008), Regional and seasonal variations in aerosol optical characteristics and their frequency distributions over India during 2001–2005, *J. Geophys. Res.*, *113*(D8), D08207, doi:10.1029/2007JD008560.
Ramanathan, V., C. Chung, D. Kim, T. Bettge, L. Buja, J. T. Kiehl, W. M. Washington, Q. Fu, D. R. Sikka, and M. Wild (2005), Atmospheric brown clouds: Impacts on South Asian climate and hydrological cycle, *Proc. Natl. Acad. Sci.*, *102* (15), 5326–5333, doi:10.1073/pnas.0500656102.
Randles, C. A., and V. Ramaswamy (2008), Absorbing aerosols over Asia: A Geophysical Fluid Dynamics Laboratory general circulation model sensitivity study of model response to aerosol optical depth and aerosol absorption, *J. Geophys. Res.*, *113*(D21), D21203, doi:10.1029/2008JD010140.
Reddy, M. S., and C. Venkataraman (2002), Inventory of aerosol and sulphur dioxide emissions from India: I—Fossil fuel combustion, *Atmos. Environ.*, *36*(4), 677-697.
Roeckner, E., et al. (2003), The atmospheric general circulation model ECHAM5. PART I: Model description, *Report Rep. 349*, 1-140 pp, Max Planck Institute for Meteorology, Hamburg, Germany.
Roeckner, E., P. Stier, J. Feichter, S. Kloster, M. Esch, and I. Fischer-Bruns (2006), Impact of carbonaceous aerosol emissions on regional climate change, *Climate Dynamics*, doi:10.1007/s00382-00006-00147-00383.
Romatschke, U., and R. A. Houze (2011), Characteristics of precipitating convective systems in the South Asian monsoon, *J. Hydrometeor.*, *12*, 3–26.
Singh, R. P., S. Dey, S. N. Tripathi, V. Tare, and B. Holben (2004), Variability of aerosol parameters over Kanpur, northern India, *J. Geophys. Res.*, *109*(D23), D23206, doi:10.1029/2004JD004966.
Soni, V. K., G. Pandithurai, and D. S. Pai (2012), Evaluation of long-term changes of solar radiation in India, *Int. J. Climatol.*, *32*, 540–551, doi:10.1002/joc.2294.
Stier, P., et al. (2005), The aerosol-climate model ECHAM5-HAM, *Atmos. Chem. Phys.*, *5*, 1125–1156.
Stier, P., J. H. Seinfeld, S. Kinne, and O. Boucher (2007), Aerosol absorption and radiative forcing, *Atmos. Chem. Phys.*, *7*(19), 5237–5261.
Tegen, I., S. P. Harrison, K. Kohfeld, I. C. Prentice, M. Coe, and M. Heimann (2002), Impact of vegetation and preferential source areas on global dust aerosol: Results from a model study, *J. Geophys. Res.*, *107*(D21), 4576, doi:10.1029/2001JD000963.

Tiedtke, M. (1989), A comprehensive mass flux scheme for cumulus parameterization in large-scale models, *Mon. Wea. Rev.*, *117*, 1779–1800.

Tompkins, A. M. (2002), A prognostic parameterization for the subgrid-scale variability of water vapor and clouds in large-scale models and its use to diagnose cloud cover, *J. Atmos. Sci.*, *59*, 1917–1942.

Tost, H., P. Jockel, and J. Lelieveld (2006), Influence of different convection parameterisations in a GCM, *Atmos. Chem. Phys.*, *6*, 5475–5493.

Tripathi, S. N., S. Dey, V. Tare, and S. K. Satheesh (2005), Aerosol black carbon radiative forcing at an industrial city in northern India, *Geophys. Res. Lett.*, *32*(L08802), doi:10.1029/2005GL022515.

Twomey, S. A. (1977), The influence of pollution on the shortwave albedo of clouds, *J. Atmos. Sci.*, *34*, 1149–1152.

Urankar, G., T. V. Prabha, G. Pandithurai, P. Pallavi, D. Achuthavarier, and B. N. Goswami (2012), Aerosol and cloud feedbacks on surface energy balance over selected regions of the Indian subcontinent, *J. Geophys. Res.*, *117*(D04210), doi:10.1029/2011JD016363.

Vadrevu, K. P., E. Ellicott, K. V. S. Badarinath, and E. Vermote (2011), MODIS-derived fire characteristics and aerosol optical depth variations during the agricultural residue burning season, north India, *Environ. Pollut.*, *159*, 1560–1569.

Venkataraman, C., G. Habib, A. Eiguren-Fernandez, A. H. Miguel, and S. K. Friedlander (2005), Residential biofuels in south Asia: Carbonaceous aerosol emissions and climate impacts, *Science*, *307*(5714), 1454–1456, doi:10.1126/science.1104359.

Venkataraman, C., G. Habib, D. Kadamba, M. Shrivastava, J. F. Leon, B. Crouzille, O. Boucher, and D. G. Streets (2006), Emissions from open biomass burning in India: Integrating the inventory approach with high-resolution Moderate Resolution Imaging Spectroradiometer (MODIS) active-fire and land cover data, *Global Biogeochem. Cy.*, *20*(2), GB2013, doi:10.1029/2005GB002547.

Vignati, E., J. Wilson, and P. Stier (2004), M7: An efficient size-resolved aerosol microphysics module for large-scale aerosol transport models, *J. Geophys. Res.*, *109*(D22), D22202, doi:10.1029/2003JD004485.

Wang, C., D. Kim, A. M. L. Ekman, M. C. Barth, and P. J. Rasch (2009), Impact of anthropogenic aerosols on Indian summer monsoon, *Geophys. Res. Lett.*, *36*(L21704), doi:10.1029/2009GL040114.